Acoustic phonons in nanowires probed by ultrafast pump-probe spectroscopy

Pierre-Adrien Mante, Laurent Belliard, Bernard Perrin

Review article

Pierre-Adrien Mante*, Laurent Belliard and Bernard Perrin

Acoustic phonons in nanowires probed by ultrafast pump-probe spectroscopy

https://doi.org/10.1515/nanoph-2018-0069
Received June 6, 2018; revised August 19, 2018; accepted August 20, 2018

Abstract: The fascinating relationship between structure and property in nanowires has enabled a wealth of applications in photonics and electronics. The behavior of phonons in nanowires is also modified compared to their bulk counterparts. In this review, we provide an overview of the recent efforts to investigate the properties of acoustic phonons in nanowires using ultrafast optical methods. In particular, we focus on the calculation of the modified phonon dispersion in nanowires and how to address them optically. We then discuss experimental investigations in arrays of nanowires and a single nanowire. The analysis of phonon behavior reveals the possibility to perform advanced mechanical characterization and to vary the thermal properties of nanowires. The review concludes with a brief perspective on future research directions, from phonon-induced control over properties to three-dimensional (3D) acoustic nano-imaging.

Keywords: acoustic phonons; femtosecond pump-probe spectroscopy; mechanical properties; nanowires.

1 Introduction

Nanowires are nanoscale materials that display confinement in two dimensions. For photons, electrons and phonons, this confinement leads to modified behavior compared to the bulk counterpart and has triggered much interest in the development of novel applications in various fields [1], such as photovoltaics [2, 3], electronics [4, 5], and biology [6, 7]. Nowadays, advanced growth methods enabling high crystallinity [8], geometric [9], and composition [10] control of nanowires are available and have enabled the investigation of novel phenomena, such as signature of Majorana fermions [11], sub-attogram sensing [12], or the quantum limit of energy conversion [13]. With always improving fabrication methods [14, 15], nanowires offer a perfect playground to further study condensed matter issues in low-dimensional systems.

Phonons play a central role in defining the properties of a material. For instance, in many materials, they are the main heat carrier and thus they determine the thermal properties. The interaction of electrons with phonons is also a critical parameter, as it plays an essential role in charge transport [16], and also in superconductors [17]. The investigation of phonons has thus attracted a lot of interest over the years. In nanowires, properties related to phonons, such as thermal conductivity, have peculiar behavior compared to bulk. With decreasing diameter, the thermal conductivity of nanowires decreases, and can even reach values 100 times smaller than when in bulk [18]. This particularity was exploited to make efficient nanowire thermoelectric devices that can convert heat into electricity [19, 20]. The origin of the decrease of thermal conductivity has been attributed mainly to two effects: increased phonon scattering due to higher surface to volume ratio and modification of the phonon dispersion relation. However, a study correlating the microscopic behavior of phonons to the macroscopic thermal properties of nanowires is still missing.

Coherent phonons are also interesting for their imaging and characterization potential [21, 22]. Electronic or optical microscopy can efficiently perform the imaging of microscopic objects. However, these techniques are limited. For instance, due to the weak penetration of electrons, electronic microscopy is limited to the study of the surface of materials. In a similar way, optical imaging in opaque materials can only give information on the surface, and the large wavelength of visible light limits the achievable resolution. Moreover, with these techniques, the source of contrast is related to the electronic structure of the materials and does not grant access to other

***Corresponding author: Pierre-Adrien Mante,** Department of Applied Physics, Hong Kong Polytechnic University, Hong Kong, Hong Kong SAR; and Division of Chemical Physics and NanoLund, Lund University, Lund, Sweden, e-mail: pierre-adrien.mante@polyu.edu.hk. http://orcid.org/0000-0002-4950-5152
Laurent Belliard and Bernard Perrin: Sorbonne Université, CNRS, Institut des NanoSciences de Paris, INSP, F-75005 Paris, France

properties, such as the mechanical properties. Acoustic imaging offers a nice alternative to overcome these limitations as phonons can propagate over long distances, may have short wavelengths up to a few nanometers, and the source of contrast comes from the acoustic impedance. However, one of the issues is the difficulty of developing small high-frequency acoustic transducers, which limits the resolution. The use of nanowires as transducers has been proposed to enable small acoustic sources [23]. However, for this purpose, and to understand thermal transport, a deeper understanding of phonons propagation in nanowires is required.

In this review, we discuss the progress that has been done to experimentally address the phononic properties of nanowires, with an emphasis on the results obtained using the picosecond ultrasonics' technique [24]. The following is organized into seven sections. First, we describe in Section 2 the behavior of phonons in nanowires with an emphasis on the method of calculation of the dispersion relations, and in particular with the xyz algorithm [25]. In Section 3, we present and discuss the interaction between photons and phonons in nanowires. In Section 4, we introduce the principles of femtosecond pump-probe spectroscopy and its application to the study of phonons. In Section 5, we depict the various investigations of phonons in arrays of nanowires, and more precisely we are interested in the study of both localized and propagating phonons. Section 6 is dedicated to the study of phonons in a single nanowire. And finally, in Section 7, we summarize the current state of our understanding of phonon behavior in nanowires.

2 Phonons in nanowires

2.1 Calculation of phonon dispersion relations in nanowires

Leo August Pochhammer was the first to tackle the question of elastic waves in a homogeneous, isotropic, cylindrically shaped object in 1874 [26]. Charles Chree independently obtained similar results in 1889 [27]. The solution to this problem for compressional waves is the Pochhammer-Chree equation which takes the following form:

$$\frac{2l}{a}(m^2+q^2)J_1(la)J_1(ma)-(m^2-q^2)^2J_0(la)J_1(ma) - 4q^2lmJ_1(la)J_0(ma)=0, \quad (1)$$

where a is the cylinder radius, J_0 and J_1 are the zero- and first-order Bessel functions of the first kind, $l=\left[\left(\frac{\omega_n}{V_l}\right)^2-q^2\right]^{\frac{1}{2}}$ and $m=\left[\left(\frac{\omega_n}{V_t}\right)^2-q^2\right]^{\frac{1}{2}}$, with ω_n, the pulsation of mode n, v_l and v_t the longitudinal and transverse sound velocity, respectively, and q, is the wave vector. This relation links the wave vector to the frequency of phonons and characterizes the dispersion of the elastic waves. The complete derivation of the Pochhammer-Chree equation is beyond the scope of this review but has been extensively discussed in multiple articles and textbooks [28, 29].

In the long wavelength approximation ($q=0$), equation (1) can be simplified [30]:

$$J_1\left(\frac{\omega_n a}{v_t}\right)\left[2\frac{v_t}{v_l}J_1\left(\frac{\omega_n a}{v_l}\right)-\frac{\omega}{v_t}J_0\left(\frac{\omega_n a}{v_l}\right)\right]=0. \quad (2)$$

The roots of the two terms of Eq. 2 define two different types of resonant modes for an infinitely long isotropic nanowire. The roots of J_1 are modes with purely axial displacement, while the solution of the second term corresponds to modes with purely radial displacement at $q=0$, such as the breathing mode.

However, the Pochhammer-Chree equation (Eq. 1) is limited to an isotropic medium, which greatly limits its application as many materials have anisotropic elastic properties. To obtain the dispersion relations of elastic waves in an anisotropic cylinder, we have to resort to numerical approaches, such as finite-element simulations (FEM) [31]. FEM simulations are very complex and require lengthy code writing, however, commercial software now offers the possibility to perform these calculations more easily.

Here, we focus on the calculation of dispersion relations of phonons in anisotropic waveguides using the xyz algorithm, also referred to as the resonant ultrasound spectroscopy (RUS) method, developed by Visscher et al. [25]. The starting point of the xyz algorithm is the Lagrangian of the system:

$$L=\int(KE-PE)dV=\frac{1}{2}\int\left[\rho\omega^2u_iu_i-C_{ijkl}\frac{\partial u_i}{\partial x_j}\frac{\partial u_k}{\partial x_l}\right]dV, \quad (3)$$

where KE is the kinetic energy and PE is the potential energy, V is the volume of the system, ρ is its mass density, ω is the angular frequency, u_i is the lattice displacement components in direction x_i, and C_{ijkl} is the elasticity tensor. Taking into account Hamilton's principle, we then obtain:

$$\delta L = \int \left[\rho\omega^2 u_i - C_{ijkl} \frac{\partial^2 u_k}{\partial x_j \partial x_l} \right] \delta u_i dV - \int n_j C_{ijkl} \frac{\partial u_k}{\partial x_l} dS = 0. \quad (4)$$

If we now consider that the nanowire is free-standing, then the stress vanishes at the boundary of the structure and the second term of the right-hand side of Eq. 4 is 0. We then end up with the Christoffel equation:

$$\rho\omega^2 u_i = C_{ijkl} \frac{\partial^2 u_k}{\partial x_i \partial x_l}, \quad (5)$$

To solve this equation, we expand the displacement in terms of a complete set of basic functions Φ_α.

$$u_i = \sum a_{i\alpha} \Phi_\alpha \quad (6)$$

The principle of the xyz algorithm resides in the choice of these basis functions, which are powers of the coordinates. In the specific case of a cylindrical nanowire of diameter r, and considering the propagation of vibrations along the z coordinate, the most convenient set of basis function takes the form:

$$\Phi_\alpha = \left(\frac{x}{r}\right)^m \left(\frac{y}{r}\right)^n e^{iqz} \quad (7)$$

With $\alpha = (m, n)$, a set of two non-negative integers and q, the phonon wavevector. We then inject Eq. 5 and 6 into Eq. 4 and finally obtain:

$$[\omega^2 E - \Gamma] a = 0 \quad (8)$$

with

$$E_{i\alpha,l\beta} = \delta_{il} \frac{\rho}{V} \int_V \Phi^*_\beta \Phi_\alpha dV, \quad (9)$$

and

$$\Gamma_{i\alpha,l\beta} = \frac{C_{ijkl}}{V} \int_V \frac{\partial \Phi^*_\beta}{\partial x_i} \frac{\partial \Phi_\alpha}{\partial x_k} dV. \quad (10)$$

The advantage of using a power series of the coordinate is the ease of classifying the calculated phonon modes. By introducing the set $(\mu, \nu) = ((-1)^m, (-1)^n)$, we can classify the modes thanks to parity considerations. The basis functions have even or odd parity for inversion of x or y coordinates. By construction, if the displacement u_z has for parity (μ, ν), then the displacements u_x and u_y have parity $(-\mu, \nu)$ and $(\mu, -\nu)$, respectively. For instance, let us assume that u_x and u_y have parity (−, +) and (+, −), respectively. Such conditions correspond to dilatational modes of the nanowire. This means that the displacement in the x-direction of the point $(-x_1, y_1)$ is equal to the

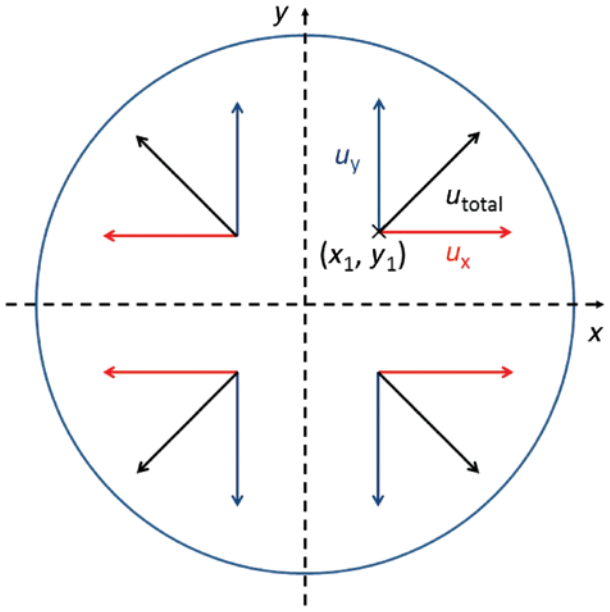

Figure 1: Parity of the displacement along x and y for the dilatational modes.
For these modes, the x- and y-axis are axis of symmetry.

displacement at $(-x_1, y_1)$, but opposite to the displacement at (x_1, y_1) as shown in Figure 1.

Using similar considerations for other parity, we can classify the modes into three categories as shown in Table 1: dilational, flexural, and torsional modes. In the following, we will discuss only dilational modes, unless otherwise specified, as these modes are the ones that have been mostly investigated.

The xyz algorithm is a versatile approach and has been widely used to obtain the phonon dispersion relations of nanowires of various cross-sections: rectangular [32], circular [33], and hexagonal [34], but also for nanowire heterostructures like core-shell [33], and superlattices [35, 36]. Furthermore, once the dispersion relations are obtained, it is possible to calculate the phonon group velocity, which is crucial to understand thermal transport [37], charge mobility [38, 39], and thermoelectric properties in nanowires [40].

Table 1: Classification of normal modes of a nanowire according to the parity of the displacements.

	u_x	u_y	u_z
Dilatational modes	(−, +)	(+, −)	(+, +)
Flexural modes	(−, −)	(+, +)	(+, −)
	(+, +)	(−, −)	(−, +)
Torsional modes	(+, −)	(−, +)	(−, −)

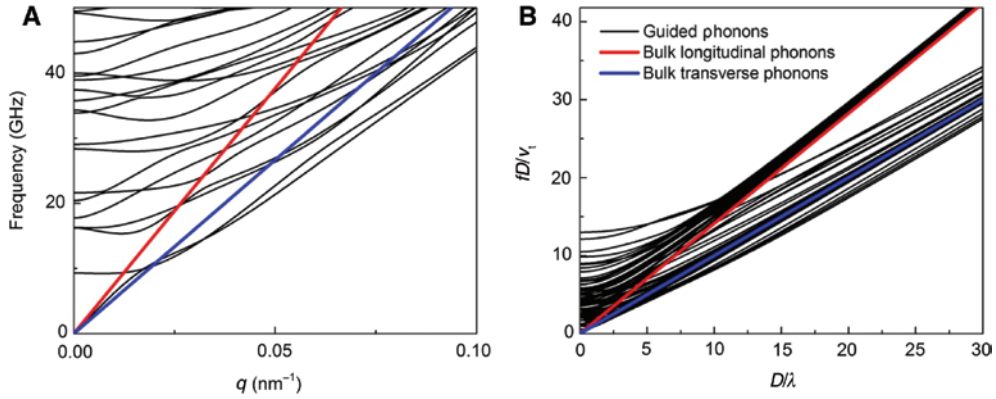

Figure 2: Phonon dispersion relations in nanowires.
(A) Phonon dispersion relations in an infinitely long GaAs nanowire of 200 nm of diameter oriented along the (100) directions (black curves) and of longitudinal (red curve) and transverse (blue curve) phonons in a bulk GaAs substrate propagating along the (100) direction for wavelength of the same order as the diameter. (B) Dispersion relations for larger wave vector displayed for a dimensionless wavevector D/λ showing the transition from confined to bulk phonons.

2.2 Phonons in nanowires vs. in bulk

We now investigate the changes in phonon behavior in nanowire compared to bulk materials in light of the dispersion relations and displacement fields calculated with the xyz algorithm. The dispersion relations of the dilatational modes of a 200 nm diameter GaAs nanowire oriented along the (100) direction are shown in Figure 2.

In a bulk material, three acoustic phonon polarizations can exist at most: one longitudinal and two transverse modes. In Figure 2A, we see that in nanowires this limitation is lifted, and numerous phonon branches can be found. The origin of these branches can be understood as follows: the confinement in two directions induces a discretization of the energy level, similar to the particle in a box model. However, along the nanowire axis, we consider that the dimensions are infinite and thus that phonons can propagate. A consequence of these considerations is that phonon branches with non-zero frequencies at $q=0$ are observed, in contrast to the phonon acoustic modes of a bulk material. Similar to the case of electrons, the confinement results in the formation of one-dimensional (1D) subbands [41].

The lowest frequency mode, which corresponds to longitudinal waves in the nanowire, has, in the long wavelength approximation, a phase velocity defined by:

$$c_0 = \sqrt{\frac{E}{\rho}}, \tag{11}$$

For a nanowire of finite length L, with large aspect ratio ($L/a >> 1$), the extensional mode of the nanowires corresponds to this mode for a wavevector given by L. It has thus been extensively used to investigate the Young's modulus of materials. For larger wavevectors, the slope of this branch decrease. This decrease is governed partly by the Poisson's ratio of the material as shown in Figure 3 [42].

If we now consider all the modes, we can see in Figure 2A that the slope of the phonon branches is smaller than the slope of bulk branches. In other words, the group velocity of phonons in nanowires is smaller than in bulk materials. This phenomenon is one of the reasons why thermal conductivity, which is the sum of the contribution of all phonons to heat transport, [43], is lower in nanowires than in bulk. Additionally, we see that for specific branches and wave vector ranges exotic behavior arises, such as negative slope, synonymous with negative group velocity [44]. Such properties could allow the

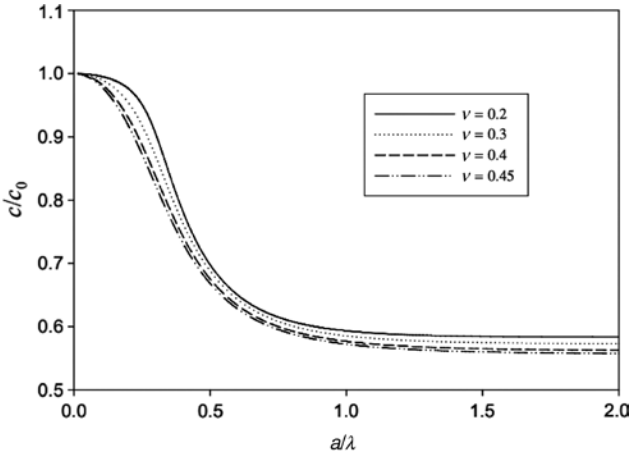

Figure 3: Dimensionless phase velocity of the longitudinal mode of a rod for various Poisson's ratio values. Reprinted with permission from [42]. Copyright (2003) Elsevier.

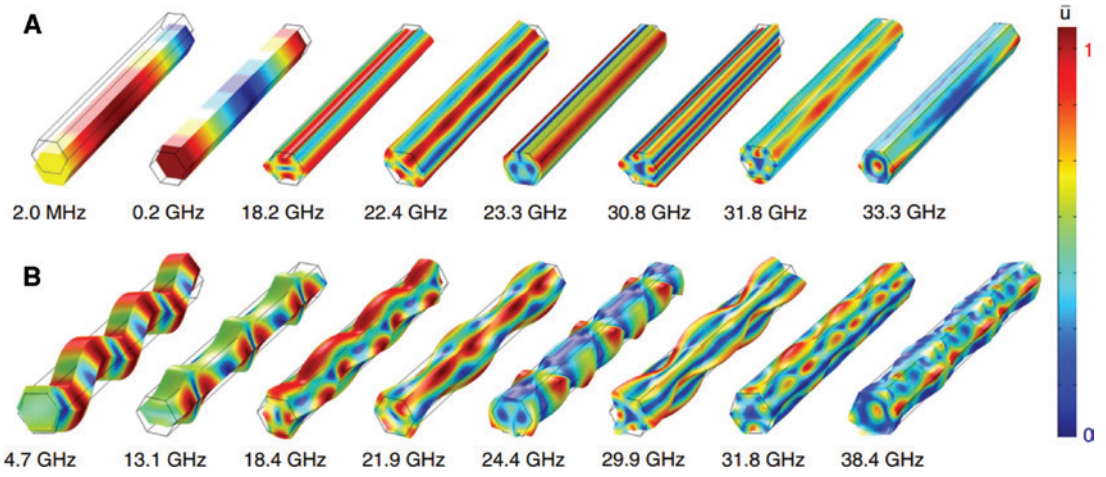

Figure 4: Normalized displacement fields for various modes of a 1 µm long GaAs nanowire for a wavevector (A) $q = 0.3\ \mu m^{-1}$ and (B) $q = 18\ \mu m^{-1}$. The dispersion relations of these modes are displayed in Figure 7. Adapted from [46].

development of acoustic metamaterials with nanowires as a building block [45].

For larger wave vectors, as shown in Figure 2B, we see that all the phonon branches group into two asymptotic limits that correspond to the bulk longitudinal and transverse phonons. In this figure, we display the dispersion curves as a function of a dimensionless wavevector D/λ, with λ the phonon wavelength. When the wavelength of phonons is on the order of or larger than the diameter (in the region $D/\lambda < 10$), phonons are strongly modified. On the other hand, when the wavelength of phonons becomes much smaller than the diameter of the nanowires, i.e. when confinement effects disappear, phonons propagate as they do in a bulk material.

In nanowires, not only the dispersion curves are modified compared to bulk, but also the displacement fields, as shown in Figure 4.

In a bulk material, only three branches of phonons are possible: one longitudinal and two transverse. For these modes, the displacement is either parallel (longitudinal phonons) or perpendicular (transverse phonons) to the direction of propagation. On the other hand, in nanowires, due to the modified boundary conditions and the cylindrical symmetry, more complex displacement patterns are observed, as shown in Figure 4. In particular, we can notice a fourth order axis symmetry induces by the cubic anisotropy of the single crystal. In polycrystalline material, this symmetry would disappear.

Overall, phonons in nanowires display features extremely different from phonons in bulk: numerous modes, non-zero frequencies at $q = 0$, non-linear dispersion and complex displacement field. However, addressing these phonons is a challenging task due to the small dimensions of nanowires.

2.3 Light and sound interaction in nanowires

In nanowires, the small dimensions, approximately 100 nm, implies that the phonons that are modified by confinement have frequencies in the sub-terahertz range. Such high frequencies are difficult to detect electronically, therefore, light is often the tool of choice.

The interaction of light with sound can take different forms [47]. First, we look at the effect of the small dimensions of nanowires, which are smaller than the dimensions of a diffraction-limited optical beam. The vibration of the nanowires is synonymous with a displacement of its boundaries, and therefore, a change of volume, especially for radial modes. How this effect influences light and sound interaction can be understood by looking at Figure 5. We consider a nanowire, with permittivity ε_a, surrounded by a medium of permittivity ε_b. When a phonon is excited, the volume of the nanowire is modified and in specific area, the light interacts with a medium of different properties and behaves differently.

Another possible light and sound interaction process is related to the photoelastic effect: the change of refractive index induced by the presence of a strain. This effect

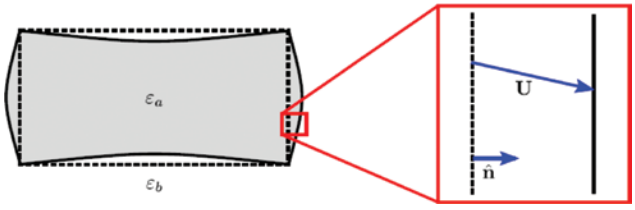

Figure 5: Illustration of the influence of boundary displacement. Reprinted with permission from [47]. Copyright (2015) American Physical Society.

is dominant in bulk materials and leads to Brillouin scattering. This scattering process occurs as follows: a photon of wave vector k_1 and frequency ω_1 interacts with a phonon of wave vector q and frequency Ω to generate a scattered photon of wave vector k_2 and frequency ω_2. For this interaction, energy and momentum conservations dictate [48]:

$$\pm q = k_2 - k_1, \tag{12}$$

$$\pm \Omega = \omega_2 - \omega_1. \tag{13}$$

The scattering of light by acoustic waves has been used extensively to study the phase transition, structural relaxation, and elastic properties of various materials [49].

In nanowires, the rules of light and sound scattering are modified due to confinement effects [47, 50, 51]. We have seen in Section 2 that confinement affects the propagation of phonons. Photons of visible light have wavelengths on the order of the dimension of confinement and therefore their dispersion is also modified [52, 53], as shown in Figure 6.

In Figure 6A, we observe resonances in the absorption of Si nanowires of various diameters. These resonances are due to the excitation of photonic eigenmodes of the nanowire. In Figure 6B, the electric field associated with the first two resonant modes of a nanowire are seen. The behavior of photons is thus similar to the one of phonon, with electric fields (displacement fields for phonons) drastically different from bulk.

The confinement in the cross-section of the nanowire induces a discretization of the energy of both photons and phonons. On the other hand, along the axis of the nanowire, photons and phonons can propagate freely. We thus have the appearance of 1D photonic and phononic sub-bands. A consequence of this effect is that phonons and photons can propagate only along the nanowire axis. In these conditions, Eq. (10) and (11) becomes:

$$q = 0 \text{ or } 2k, \tag{14}$$

where we have considered that Ω is small compared to ω_1 and ω_2, and as a consequence, $k_1 \approx k_2 \approx k$. This expression stems from the fact that scattered light has to be collinear with the incident light, and can thus be either forward scattered or backward scattered [50]. We see that it then becomes possible to study resonant phononic modes ($q = 0$) through forward scattering, and propagating phonons ($q = 2k$) with backward scattering.

When the light intensity is sufficiently strong, we enter a second regime: stimulated Brillouin scattering (SBS). In Brillouin scattering, light interacts with the thermally generated phonon population. On the other hand, in SBS, the incoming light interacts with the medium, generally through electrostriction, which leads to the coherent generation of phonons [54]. The light can then interact with these phonons. SBS is often considered as a parasitic effect in optical fiber communication [55] but was also used to show the modifications of phonon modes due to confinement in these structures [56]. However, in recent years, a renewed interest in SBS developed due to the possibility to use this effect for the investigation of various physical effects, such as Brillouin induced transparency [57] or cooling [58]. In nanowires, the confinement of light and sound induce an enhancement of their interaction,

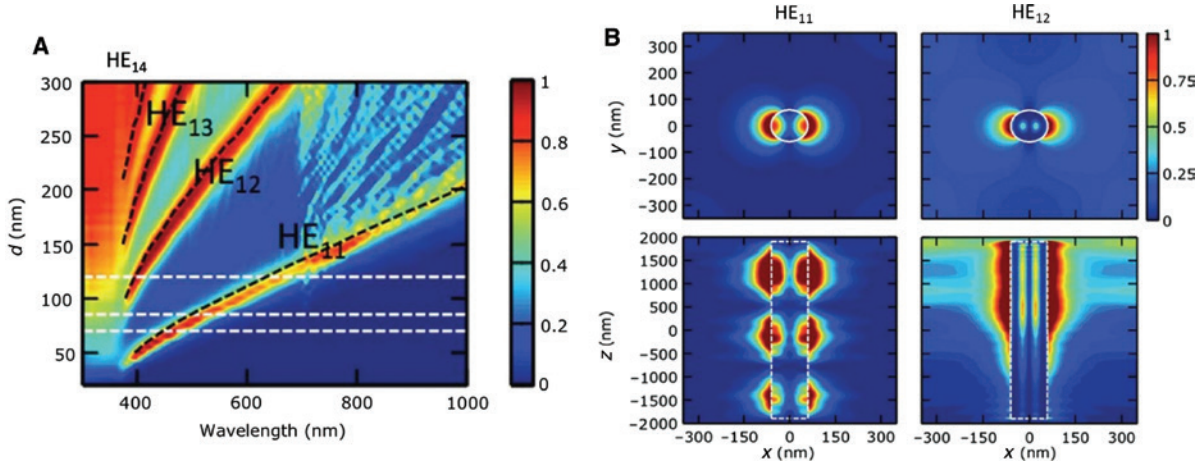

Figure 6: Optical modes of a nanowire.
(A) Contour plot of absorption as a function of photon wavelength and nanowire diameter for vertical Si nanowire arrays. (B) Electric field intensity plots of the optical mode of a 120 nm diameter Si nanowires at a wavelength of 670 and 400 nm, which correspond to the HE_{11} (left side) and the HE_{22} (right side), respectively. Reprinted with permission from [53]. Copyright (2012) Optical Society of America.

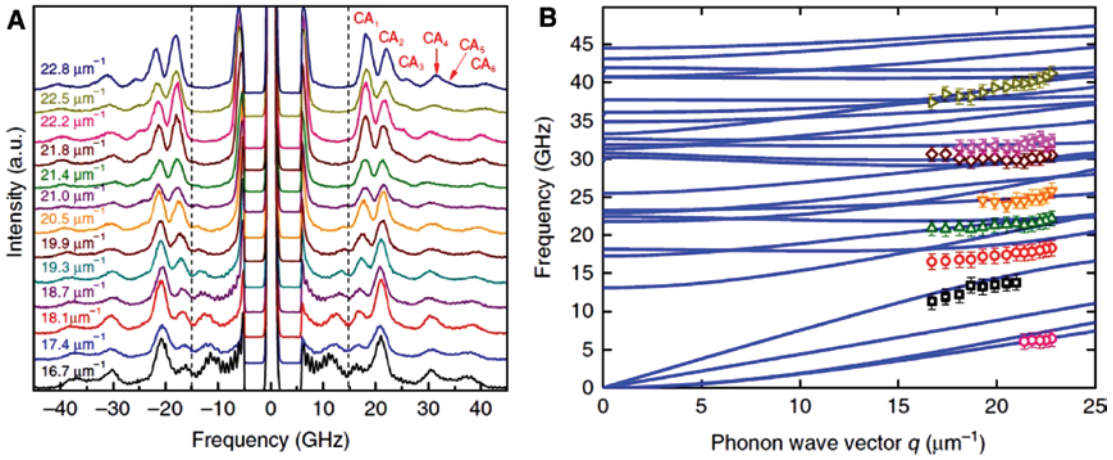

Figure 7: Brillouin scattering of nanowires.
(A) Brillouin spectra of 122 nm diameter GaAs nanowires at different optical wavelength. (B) Phonon dispersion relation of 122 nm and experimentally obtained frequencies. The dispersion relations include both the dilatational, torsional and flexural modes. Adapted from [46].

namely of electrostriction and radiation pressure, by multiple orders of magnitude [51, 59]. The possibilities offered by this enhancement are multiple and in particular, it will enable the manipulation of light by sound at the nanoscale. However, here we are interested in studying phonon behavior in nanowires, and a review of SBS in these structures is beyond the scope of this article. Interested readers should read the work of the Bahl's group [60], the Rakich's group [61], or the Eggleton's group [62].

We now look at the experimental study of phonons in nanowires using light scattering. The first observation of guided phonons in nanowires using Brillouin light scattering was performed in 2012 [63]. Unfortunately, due to the large dispersion in the diameter of the studied nanowires, the uncertainty of the measurements was very large. More recently, using the same experimental method, Kargar et al. have been able to observe confined acoustic phonons in GaAs nanowires as presented in Figure 7 [46].

In this work, they studied Brillouin scattering in GaAs nanowires, by varying the angle of incidence of light. By varying the angle, they change the wave vector of light, and, according to Eq. 12, the wave vector of the probed phonons. In this way, they were able to observe the appearance of novel modes compared to bulk materials and to reproduce the dispersion relations of confined acoustic phonons.

3 Phonon with ultrafast pump-probe spectroscopy

We have seen that Brillouin scattering is a powerful approach to study phonons. However, in the case of nanowires, some hurdles make its implementation tricky. First, no manipulation of phonons is possible, i.e. we do not have any experimental method to control the phonon population. Indeed, the accessible phonons are thermally populated and it is impossible to isolate a specific mode. SBS offers higher control over the phonon population, but it requires long interaction length, on the order of few centimeters [59]. Additionally, it is difficult to separate Brillouin scattered light from Rayleigh scattered light, which becomes an important issue for low-frequency phonons. Finally, Brillouin scattering is an experimental method in the frequency domain and thus cannot be used to study the real-time propagation of phonons. To overcome these limitations, the picosecond ultrasonics (PU) technique [24, 64], which is based on femtosecond pump-probe spectroscopy (Figure 8), is well suited.

In PU, the absorption of a femtosecond laser pulse, the pump, promotes electrons from the valence to the conduction band, as seen in Figure 8B. In a solid, electrons are responsible for the binding between atoms, and the transition of electrons from the valence to the conduction band modifies this bond and induces a displacement of atoms, thus creating a stress σ_{DP}. This mechanism of stress generation is often referred to as the deformation potential mechanism [64]. If the energy of the pump photons is larger than the band gap of the semiconductor, electrons have excess energy that they yield to the lattice by emitting phonons. The temperature of the lattice increases and, due to thermal expansion, a stress σ_{TE} is created. For most semiconductors, these two mechanisms are the most common for the creation of a stress by the absorption of a femtosecond pulse. In the case of metals, where there is no bandgap, only the thermoelastic mechanism

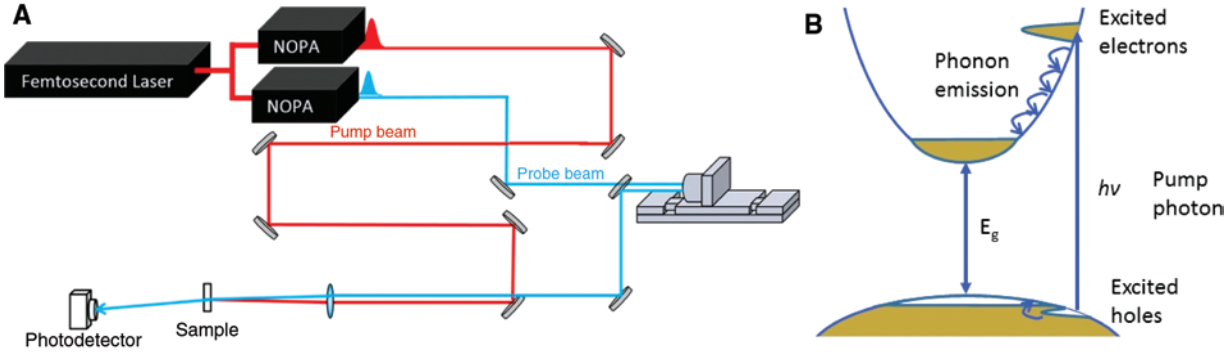

Figure 8: Pump-probe spectroscopy.
(A) Experimental pump-probe setup enabling the study of coherent phonons in the time domain. (B) Photoinduced dynamics of electrons and phonons in semiconductors. Adapted from [16].

plays a role in phonon generation. However, additional mechanisms can occur, such as piezoelectricity [65] or electrostriction [66]. These external stresses lead to the generation of strain or phonons that propagates within the semiconductor [67]:

$$\rho\frac{\partial^2 u_i}{\partial t^2}=\frac{\partial \sigma_{ij}}{\partial x_i} \tag{15}$$

with ρ, the mass density, u_i the displacement in direction i. The various phonon generation mechanisms can be further classified according to the type of driving they induce: percussive or impulsive. The heaviside function (step function) represents percussive generation mechanisms. Thermoelastic and deformation potentials are percussive, as the effect that induces the phonons, temperature increase or inter-band transition, lasts longer than the buildup of the coherent phonons. On the other hand, the Dirac function can describe impulsive mechanisms, where the duration of the driving force is much shorter than the buildup time of the coherent phonon, as in the case of electrostriction or piezoelectricity, if no screening effects are involved.

The generation of coherent phonons in nanowires follows the same rules as the ones we just described for bulk materials. However, it is crucial to also take into consideration the geometry of the sample to understand which phonon modes are generated. As seen in Figure 6, for a linearly polarized light, the electric field in the nanowire has a twofold symmetry. We thus expect the density of photoexcited carriers to have a similar symmetry. Consequently, only phonons with similar or lower symmetry, i.e. twofold or axial symmetry, should be generated [50]. However, electronic and thermal diffusion will homogenize the stress in the nanowire and the relative amplitude of twofold and axisymmetric modes is difficult to predict.

Using a second femtosecond laser pulse, the probe pulse, which can be time delayed with respect to the pump pulse, we can follow the temporal evolution of the coherent phonons within the material. The presence of strain in a material locally modifies the optical properties through the photo-elastic effect. The change of reflectivity, ΔR, induced by a phonon can thus be expressed as [24]:

$$\Delta R(t)=\int_0^\infty \eta(z,\,t)f(z)dz, \tag{16}$$

where $\eta(z,\,t)$ is the propagating strain and $f(z)$ is a sensitivity function defined by:

$$f(z)=f_0\left(\frac{\partial n}{\partial \eta}\sin\left(\frac{4\pi nz}{\lambda}-\phi\right)+\frac{\partial k}{\partial \eta}\cos\left(\frac{4\pi nz}{\lambda}-\phi\right)\right)e^{-\frac{z}{\xi}}, \tag{17}$$

with

$$f_0=8\frac{\omega[n^2(n^2+k^2-1)^2+k^2(n^2+k^2+1)^2]^{1/2}}{c[(n+1)^2+k^2]^2}, \tag{18}$$

and

$$\tan(\phi)=\frac{k(n^2+k^2+1)^2}{n(n^2+k^2-1)^2}. \tag{19}$$

$\partial n/\partial \eta$ and $\partial k/\partial \eta$ are the photo-elastic coefficients; $n+ik$ is the complex refractive index, λ is the wavelength in free space and ξ is the penetration depth of the probe light. To better understand the capabilities of this experimental technique we can isolate two cases: transparent materials and absorbing materials.

In the case of transparent materials, the detection mechanism is similar to Brillouin scattering (Figure 9A). The probe pulse arriving on the sample is partially reflected and transmitted at the free surface of the sample. The transmitted part then propagates in the sample and

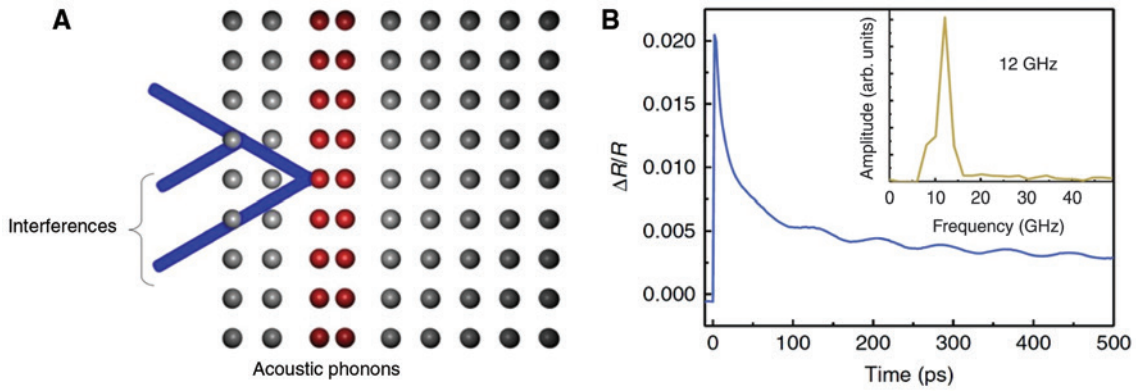

Figure 9: Coherent phonons detection.
(A) Scheme representing the detection mechanism of coherent acoustic phonons using femtosecond light pulses. (B) Transient reflectivity signal obtained on $CH_3NH_3PbI_3$ and revealing oscillations due to propagating coherent acoustic phonons. Inset: Fourier transform of these oscillations. Adapted from [16].

is backscattered by the coherent acoustic phonon pulse. The part of the pulse reflected by the free surface and the part backscattered by the acoustic phonons interfere constructively or destructively as a function of the path difference, i.e. of the position of the acoustic phonon in the sample. As a consequence, the transient reflectivity oscillates at a frequency given by $f = 2nv/\lambda$, where n is the refractive index at the probe wavelength λ, and v is the sound velocity [68].

A typical example of such a signal is shown in Figure 9B [16]. At time 0, a sharp rise of reflectivity is observed corresponding to the absorption of the pump pulse. The signal then decays due to electron-phonon scattering and charge recombination. Brillouin oscillations are seen on top of this signal. By performing the Fourier transform, we can extract the frequency of these oscillations and obtain the sound velocity, assuming the refractive index of the material. PU can thus be used to extract the sound velocities of a material and its elastic constants.

In absorbing materials, such as metals, the penetration depth of light is smaller than a few tens of nanometers. The signal will thus not appear as exponentially decaying oscillations. Instead, a small change of reflectivity is observed when the phonons are close to the surface. This can be easily seen in Figure 10 [69].

In this experiment, a 22-nm Al thin film is deposited on top of a stack of multiple materials, composed of Si_3N_4, W, and a Si substrate. Due to the strong absorption of Al, phonons are only generated and detected in this film. We can thus observe the generation of phonons in the Al film at early time scale (first 20 ps), then phonon propagates in the 500 nm thick Si_3N_4 film, are reflected at the interface with W and propagates back towards the Al film. At 135 ps, a change of reflectivity is detected corresponding

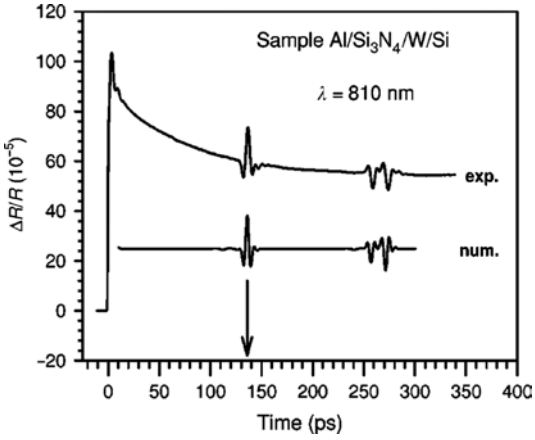

Figure 10: Transient reflectivity signal obtained on an $Al/Si_3N_4/Si$ substrate. Reprinted with permission from [69]. Copyright (2003) by The American Physical Society.

to the reentrance of the phonons in the Al film. Such signals are called echo, as they correspond to a round trip of phonons in the material. For this reason, PU is often referred to as sonar at the nanoscale. At 270 ps, a second echo is observed. This second one is caused by a second round trip in the Si_3N_4 film, but also by a round trip in the Si_3N_4/W stack. We can thus retrieve the round trip time of phonons in each layer. Assuming the value of sound velocity is known, the thickness of the thin film can be obtained from the round trip time [70].

Over the years, the PU technique has been applied to study the generation of coherent acoustic phonons in various structures, from quantum wells [71] and superlattices [72] to quantum dots [73]. In addition to the capabilities of this technique for metrology [70], it allows the investigation of the complex interactions between photons, phonons, and electrons [16, 74].

4 Phonon in arrays of nanowires

Bottom-up and top-down are the two main approaches to synthesize nanowires. Usually, top-down approaches, such as etching, lead to a rougher surface and thus bottom-up synthesized nanowires are preferred for the study of phonons. With this method, nanowires, standing on a substrate, with well-defined geometric properties and few defects can be obtained. Here, we will review some of the recent observations of phonons in such nanowires using PU. However, the vibrations of plasmonic nanorods will not be discussed here. Interested readers should consult the numerous references on this topic [75, 76].

4.1 Resonant modes

The first investigation of free-standing nanowires with PU dates back to 2007 and 2008 [77, 78]. In this work, bismuth nanowires of 200 nm diameter were investigated. The transient reflectivity signals obtained on this sample is shown in Figure 11.

In Figure 11A, two types of oscillations are observed. High-frequency phonons disappear on a very short timescale of a few ps. This signal is attributed to optical phonons and is beyond the scope of this review. On a longer timescale, another oscillation with a larger period is seen. The Fourier transform of this signal, which is shown in Figure 11B displays two peaks corresponding to these two phonon modes. The mode at 9.5 GHz is attributed to the breathing mode of the nanowires. The frequency of this mode can be calculated from Eq. 2, and the authors obtained a frequency of 7.75 GHz, on the same order as what they observed experimentally. This discrepancy of almost 20% does not allow an unambiguous attribution to the breathing mode, and further diameter-dependent experiments would have been required. However, this work was a demonstration of the possibility to address acoustic vibrations in nanowires using PU.

Following this work, multiple groups investigated the vibrations of periodic arrays of nanowires fabricated by top-down and bottom-up approaches [79, 80]. With the development of better experimental growth methods, smaller dispersion in size of the nanowires was achieved, increasing the reliability of the frequency extraction in these experiments. In Ref. [79], Chen et al. did a systematic investigation of the frequency of vibration as a function of the nanowire diameter (Figure 12).

In this work, they showed that the main frequency that is detected in periodic arrays of nanowires with PU does not depend on the period of these arrays or on the aspect ratio of the nanowires, but solely on the diameter of the nanowires. These dependencies confirm that the observed oscillations are vibrations of the nanowires. By comparing the experimentally obtained frequencies to the expected frequencies calculated using Eq. 2, they were able to show that the dominant frequency corresponds to the breathing mode. The predominance of this mode can be understood from the fact that this is the most symmetric vibrational mode of the structure and that the diameter of the nanowires is much smaller than the laser spot size, which means that the energy deposited is uniform in the nanowire.

To observe different vibrational modes of nanowires different experimental conditions are required. In Ref. [81], a probe energy smaller than the band gap of the nanowire material was used. In that case, the probe light is partially reflected by the top surface of the nanowire, and by the

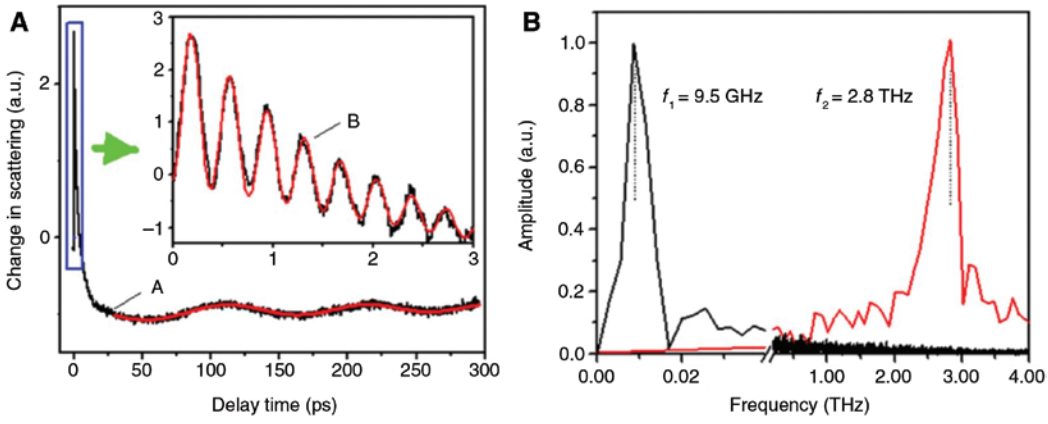

Figure 11: Coherent phonons in Bismuth nanowires.
(A) Transient reflectivity signals obtained on Bi nanowires. Inset: Zoom in on the first picoseconds of the signal. (B) Spectral analysis of the oscillating portions of the signal. Reproduced from [78], with the permission of AIP Publishing.

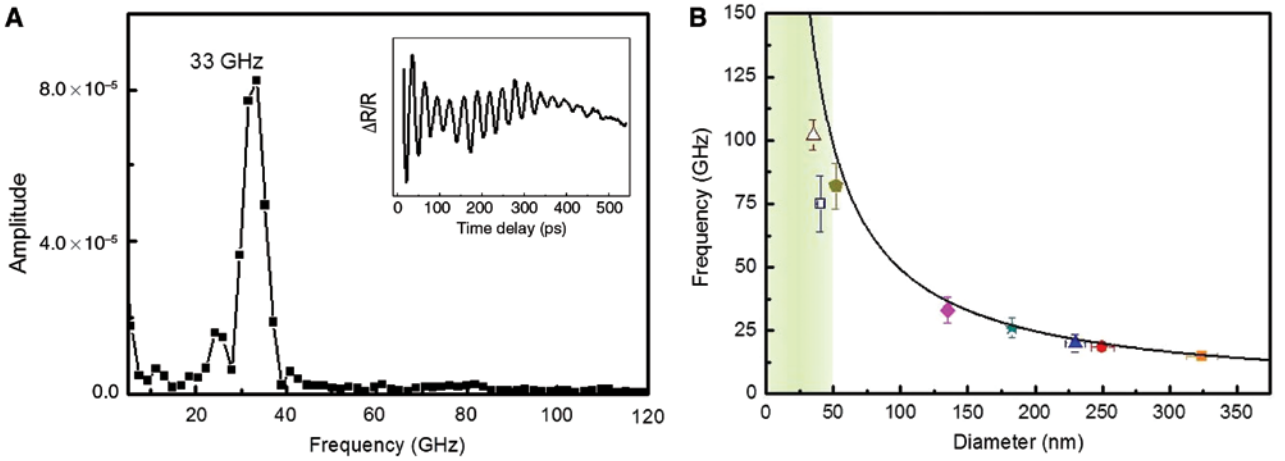

Figure 12: Breathing modes of GaN nanowires.
(A) Fourier transform of the transient reflectivity signal obtained on 135 nm diameter GaN nanowire. Inset: transient reflectivity signal after removal of the electronic contribution of a 135 nm diameter GaN nanowire. (B) Frequency of the observed oscillations as a function of the diameter of the nanowire. The black line is the result of the calculation of the breathing mode frequency using Eq. 2. Reproduced from [80].

nanowire/substrate interface. The nanowires thus act as a Fabry-Perot cavity and the reflection coefficient depends on the thickness of the cavity. Then if the absorption of the pump beam generates modes that change the length of the nanowires, it becomes possible to detect them. Using this experimental approach, the fundamental and two higher order extensional modes of GaN nanowires were observed (Figure 13). Comparison with FEM simulations confirmed the nature of these modes and revealed that the mechanical properties of GaN in nanowires remained similar to the ones in bulk.

In addition to the investigation of the confined vibrations of nanowires using visible probe light, resonant modes of standing nanowires have also been addressed with an X-ray probe [82]. In these experiments, light is not scattered by the acoustic phonons themselves, but is diffracted by the periodic plane of atoms constituting the nanowire. When coherent phonons are excited in the material, due to the absorption of the visible pump light, the lattice spacing is modulated at the phonon frequency and the diffracted signal too. With this method, researchers have been able to observe, in addition to the extensional modes of the structures, the flexural modes of the nanowires (see Table 1) that have not been detected yet with PU.

5 Propagative modes

Multiple groups have thus been interested in using the picosecond ultrasonic method to address the vibration of nanowires [77–81]. They have had some success in retrieving resonant acoustic modes of such structure, but the observation of propagating modes remained elusive. The difficulty to address propagative modes is especially detrimental to the understanding of thermal transport in semiconductor nanowires as phonons are the main heat carriers in these samples.

To make the generation and detection of propagating phonons in nanowires easier, researchers have used external transducers [23, 83, 84]. While in a pure nanowire, generation, propagation, and detection of phonons occur at the same place, which makes it difficult to separate propagating and non-propagating modes, the inclusion of a spatially distinct structure to generate and detect phonons allow the observation of propagating modes. Indeed, in these conditions, resonant modes and propagating modes will have different temporal evolutions. The most straightforward example of this concept has been achieved by incorporating a gold particle at the tip of a nanowire, as seen in Figure 14. In these experiments, the pump light is absorbed by the gold particle, which generates phonons that propagates along the nanowire, are reflected at the nanowire/substrate interface and propagates back towards the gold particle (Figure 14A).

In Figure 14B, we can see the experimental signal obtained on a 720 nm long GaAs nanowire with a diameter of 230 nm and a gold particle of 30 nm of thickness after removal of the electronic contribution. The signal generated by the gold particle can be observed on an early timescale and disappear after 300 ps. After 600 ps, the signal increases again, and the same pattern happens between 600 and 1200 ps. This periodic change of the signal is attributed to round trip of acoustic phonons in

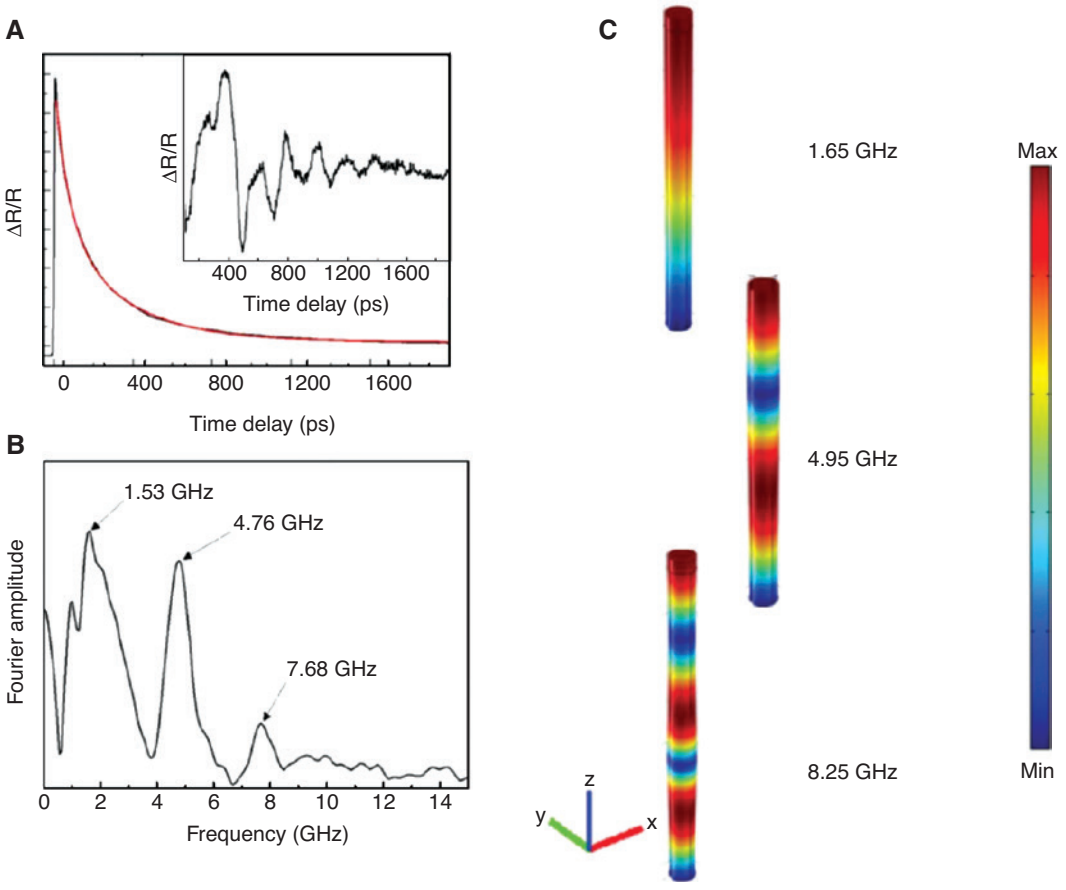

Figure 13: Extensional modes of GaN nanowires.
(A) Transient reflectivity trace with a pump wavelength of 360 nm and a probe wavelength of 720 nm obtained on 100 nm diameter and 1150 nm long GaN nanowires. (Inset) Transient reflectivity with background removed. (B) Fourier transform of transient reflectivity. (C) Normalized displacement fields of the three first extensional modes obtained by FEM simulations. Reproduced from [81].

the nanowire. By simulating the effect of such roundtrips on the signal (Figure 14C), the sound velocity of these phonons is extracted.

More advanced external transducers offer the added possibility to investigate phonon propagation in nanowires. This is the case for superlattices, a periodic stacking of two different materials. Due to this periodicity, D, a folding of the dispersion relations in a mini-Brillouin zone occurs [23, 36]. In Figure 15A, the phonon dispersion relations of 75 nm diameter GaN and AlN nanowires are shown.

GaN and AlN both have a wurtzite crystalline structure and the dispersion relations are thus similar (Figure 15A). But, as AlN has larger elastic constants, the curves are shifted towards higher frequencies. In a superlattice, the dispersion relations are folded. This phenomenon is important for the investigation of guided acoustic phonons in nanowires, as shown in Figure 15B.

As we have seen in Section 3, light and sound interactions in nanowires occur for specific conditions, namely $q=0$ or $q=2k$. To investigate the propagation of acoustic phonons, we care about the conditions where the wave vector of phonons is non-zero, i.e. $q=2k$. However, this means that for a given wavelength, a mode can only be observed at a specific wave vector, and consequently at one specific frequency, which makes it difficult to address the dispersion of phonon branches. But thanks to superlattices, and the accompanying folding, there exist multiple phonon wave vectors of the same mode that satisfies the condition $q=2k$.

Using an AlN/GaN superlattice, for the generation and detection of phonons, on top of a GaN nanowire, the round trip time as a function of the phonon frequency was investigated (Figure 16) [23].

In the upper part of Figure 16, the experimental trace, as well as curves obtained after applying a bandpass filter centered around the two lowest frequencies verifying $q=2k$ are seen. For both filtered data, a component is seen at an early time scale, corresponding to the generation of phonons within the superlattice. For the 15 to 40 GHz filter, the signal reappears after 300 ps, and for the 53 to 64 GHz, the signal

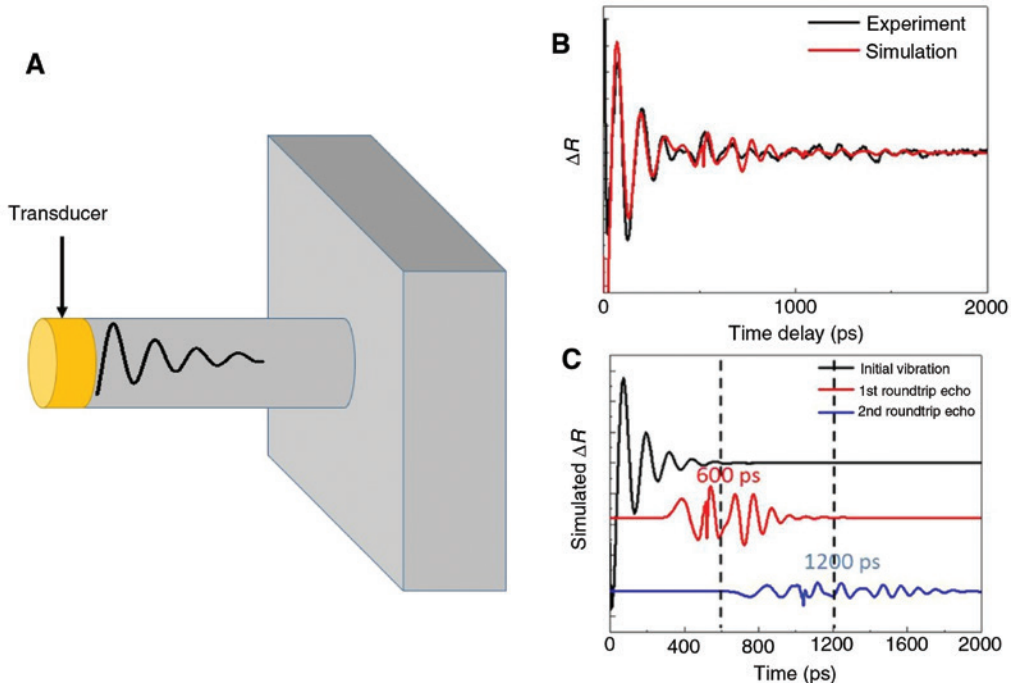

Figure 14: Propagation of phonons in a nanowire.
(A) Schema representing the experimental conditions to allow the observation of propagating modes with an external transducer. (B) Transient reflectivity obtained a 720 nm long GaAs nanowire with a diameter of 230 nm and a gold particle of 30 nm of thickness after removal of the electronic contribution and simulation. (C) decomposition of the simulated signal highlighting the multiple round trips made by the phonons in the nanowire structure. Adapted from [83], with the permission of AIP Publishing.

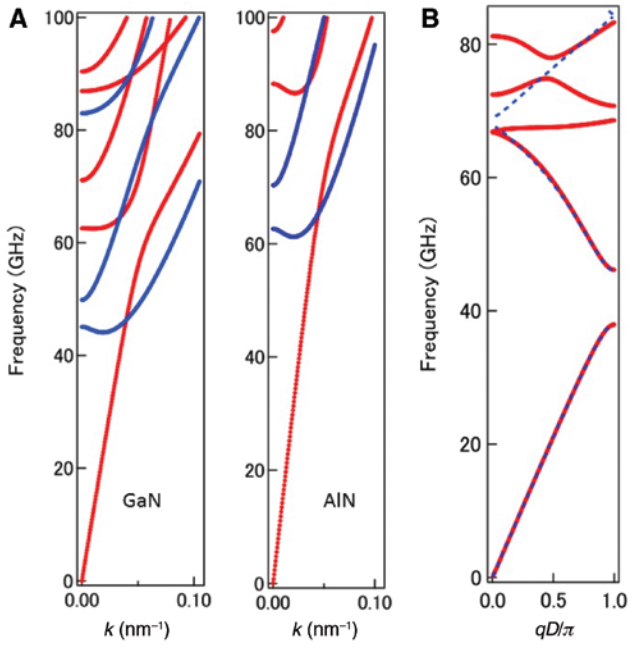

Figure 15: (A) Phonon dispersion relations of a 75 nm diameter GaN and AlN nanowires. (B) Dispersion relations of an AlN/GaN nanowire superlattice with a 56 nm GaN thickness and 42 nm AlN thickness. Reproduced from [36]. Copyright 2018 The Japan Society of Applied Physics.

reappears at 500 ps. The reappearing signal corresponds to the round-trip of phonons within the nanowire, and the difference in round trip time is reflecting the different velocities at different frequencies. In Figure 17A, we reported the measured sound velocities on the calculated frequency dependent group velocity of 75 nm GaN nanowires.

We observe a good agreement between the experiments and the calculation, confirming the modified dispersion in nanowires. This result is important to understand the decreased thermal conductivity of nanowires [18] and the possibilities it offers for thermoelectrics [19, 20]. The velocity of phonons in nanowires is strongly decreased compared to bulk (Figure 17B). As the thermal conductivity is directly related to the group velocity [43], this decrease partially explains the reduction of conductivity. For efficient thermoelectric devices, low thermal conductivity is needed. Using nanowires is thus a valid approach. In this structure, it is possible to further decrease the thermal conductivity, in addition to the intrinsic reduction due to confinement. Using superlattices, we have seen that phonon dispersion relations are folded in a mini-Brillouin zone. This folding leads to the formation of phononic band gaps in which the propagation of phonons is forbidden (Figure 17B). The

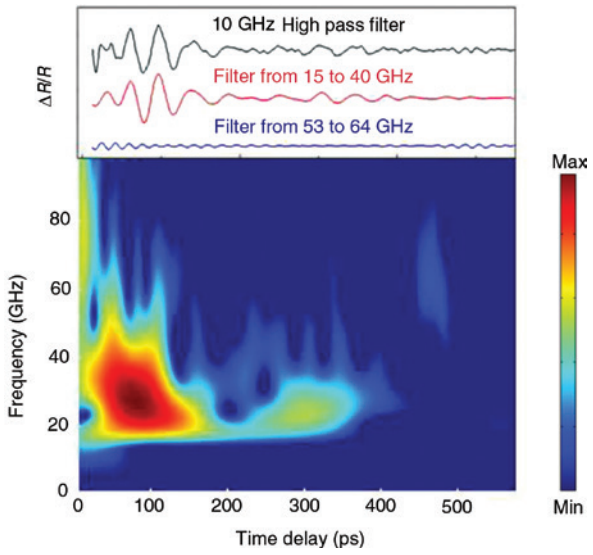

Figure 16: Top: Transient reflectivity obtained with a 360 nm pump and 720 nm probe wavelengths on a 5 periods GaN/AlN nanowire superlattices with a 56 nm GaN thickness and 42 nm AlN thickness, on top of a 900 nm long GaN nanowire with a diameter of 75 nm. with the envelope of the acoustic pulse filtered out (black curve), with a filter centered at 25 GHz (blue curve) and a filter at 60 GHz (red curve). Bottom: Time frequency analysis of the transient reflectivity with the envelope filtered out. The figure displays the amplitude of the signal at a given frequency and time. Reprinted with permission from [23]. Copyright (2013) American Chemical Society.

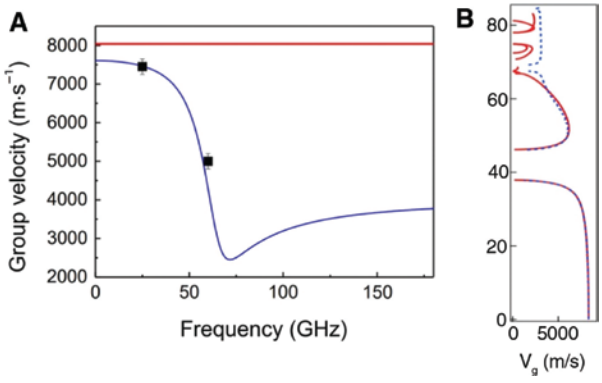

Figure 17: Group velocity in nanowire and nanowire superlattices. (A) Experimentally determined group velocities (black squares) and group velocity calculated for a 75 nm GaN nanowire (blue curve), and group velocity in bulk GaN (red curve). (B) Group velocity in an AlN/GaN superlattice. Reproduced from [36]. Copyright (2018) The Japan Society of Applied Physics.

averaged group velocity is then further decreased, and so is the thermal conductivity.

The first observations of propagating modes occurred using a dissimilar material for both the detection and the propagation of phonons. However, the study of light and sound interaction (Section 3) shows that it should be possible to detect propagating modes in nanowires [47, 50, 51]. The method in order to achieve this goal is to vary the wavelength of the probe, change the wave vector of the probed phonons (Eq. 12). In Figure 18, the Fourier transforms of the transient reflectivity signals obtained on an array of 180 nm diameter InP nanowires for two different wavelengths are shown.

When the probe wavelength is modified, some modes remain unchanged (green arrows), while other modes vary (red and blue arrows). These behaviors correspond to forward and backward scattering of the probe light by resonant and propagating modes, respectively. We also notice that only modes with twofold and axial symmetry are generated as expected from the symmetry of the electric field in the nanowire [50]. Similarly to the case of eigenmodes, i.e. non-propagating modes, similar results were obtained by using an X-ray probe instead of visible light [86].

One interesting aspect of the observation of both resonant and propagating modes is the possibility it opens for mechanical characterization. Indeed, the dispersion relations of phonons are fully determined by the elastic tensor of a material, and the diameter of the nanowire. Therefore, if it is possible to obtain experimentally more frequencies than there are independent elastic constants, complete mechanical characterization of a material is achievable. In Figure 18B, we reproduced the fitted dispersion relations of phonons using experimentally determined frequencies for GaAs nanowires [85]. As the material has the zinc-blende crystalline structure, and therefore only have three independent elastic constants, it was possible not only to fully determine the mechanical properties, but also the diameter of nanowires. Additionally, the mechanical properties of wurtzite GaAs, a phase only stable at the nanoscale were measured for the first time using this approach [85].

6 Single nanowire experiments

6.1 Resonant modes

In order to increase the signal to noise ratio, the measurements are generally performed on a large number of nanoparticles. Nevertheless, even if the elaboration processes are nowadays more and more controlled, the vibrational response is always strongly affected by the inherent size and shape distribution of the nanoparticle ensemble, which leads to inhomogeneous broadening of the signals.

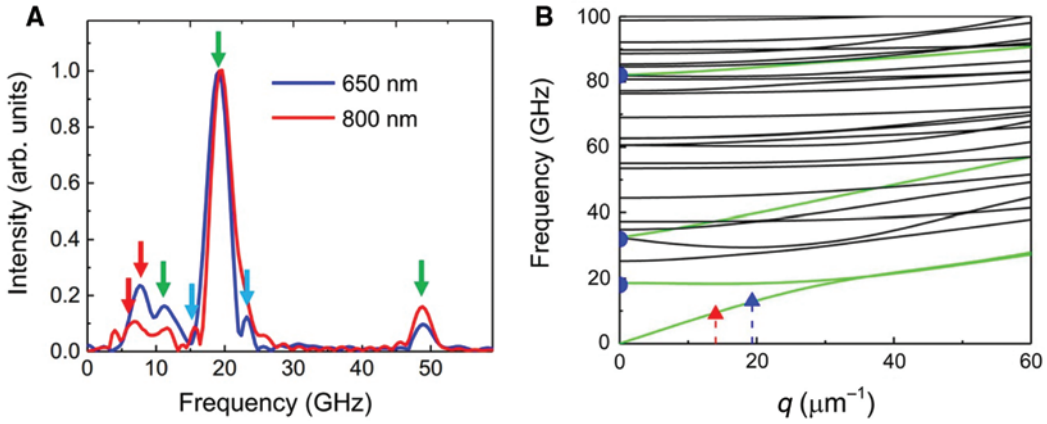

Figure 18: Scattering of light by phonons in nanowires.
(A) Normalized Fourier transform of the transient reflectivity traces obtained with a pump wavelength of 550 nm and probe wavelength of either 650 or 800 nm. The green (red and blue) arrows points at the frequencies that are unchanged (changed) with varying probe wavelength. Reprinted with permission from [50]. Copyright (2016) by The American Physical Society. (B) Experimentally obtained frequency of phonons of a GaAs zinc-blende nanowires and the fitted phonon dispersion relations. Reprinted with permission from [85]. Copyright (2016) American Chemical Society.

To overcome this drawback, recent measurements on single nanoparticles have been reported. Time-resolved measurements performed on a single nano-object require facilities based on optical mapping [87] to locate the sample and the use of objective with high numerical aperture to excite and collect the optical transient response of the selected object.

Different elaboration methods are suitable to create long single nanowire. Single-crystalline nanowires may be grown by physical vapor deposition [88] or by PVP-mediated polyol process [89]. Beyond the real interest to elaborate well-organized crystalline structure such objects generally exhibit complex cross-section and non-constant size. The template method is an alternative elaboration process based on electrodeposition in etched ion-track membranes [90]. A 30-μm thick polycarbonate foils (Makrofol, Bayer, Leverkusen, Germany) is irradiated with GeV Au^{25+} accelerated ions. Each ion creates a damaged cylindrical zone along its trajectory through the foil called latent track. After irradiation, these tracks were selectively etched in a 6 M NaOH solution at 50°C resulting in cylindrical smooth nanochannels with tunable diameter used as a template to the electrochemical growing. The main advantage is to get perfect cylindrical nanowires with constant diameter. In all the cases, the final step consisted in drop-casting the objects on the surface of the substrate (Figure 19).

As the pioneer work of van Dijk et al. [91] which investigated the dynamic response of gold nanospheres using PU, a large variety of materials and particle shape has

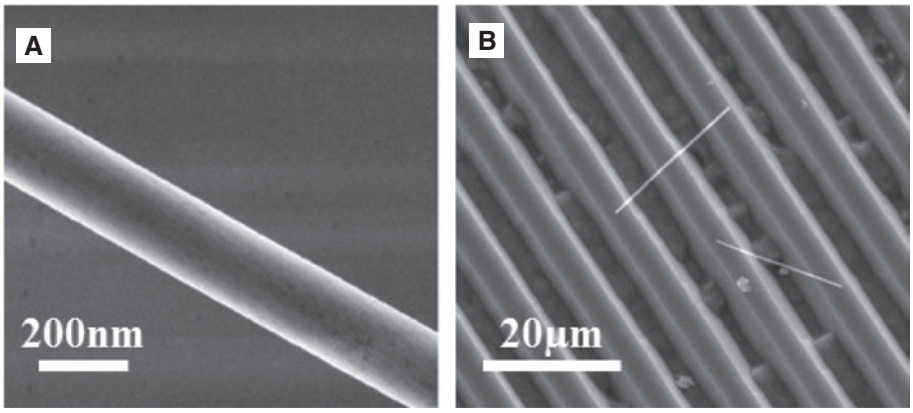

Figure 19: Single nanowire on a trench.
(A) Smooth copper nanowire supported on flat silicon substrate. (B) Two nanowires crossing pyramidal trenches etched on the silicon substrate.

been investigated like nanoprisms [92], nanowires [93], nanorings [94, 95], nanocubes [96], nanorods [75, 97], dimer nanoparticles [98] and nanoparticles [99]. All these results have been obtained by measuring the transient absorption signature, in transmission geometry using a high numerical aperture objective to recollect a maximum of light. Moreover, few results have been recently reported on reflectivity configuration in near [100–102] and far field [103–105]. In general, the vibrational modes observed are assigned to breathing modes of the structure. According to the particle shape, especially in the nanorod case, additional extensional or flexural signatures have been also reported [75, 76, 106].

The common denominator of all these previous studies is the clear evidence that particle coupling with the local environment leads to a huge damping rate. The particle-substrate interaction is at the origin of the acoustic energy transfer into the substrate. As a direct consequence, the resonator exhibits a low quality factor, defined by the energy stored over the energy lost in one cycle. In order to get insight into the energy relaxation process, across the particle surface, different routes have been investigated. In the case of particles embedded in a glass matrix [107], the increasing hydrostatic pressure obtained with the diamond anvil cell technology [108] has demonstrated a huge effect on the damping rates [107]. Additionally, the lifetime of nano-ring vibrations has been reduced by immersion in a glycerol solution [94]. In both cases, additional relaxation channels contribute to reducing the acoustic confinement into the nanoparticles thus revealing broad peaks on the Fourier spectrum, even if the measurements are performed on a single nanoparticle. Consequently, a fine estimation of the elastic properties could be very challenging. Indeed, in previously cited works dedicated to single nanowire investigations, only the fundamental breathing mode has been mentioned. Therefore, even in the simplest case of an isotropic elastic tensor, it is impossible to extract the two unknown elastic parameters (v_l and v_t) and the size of the nanowire. Even if the size is well known, using additional shape investigations based on scanning electron microscopy (SEM), we may find infinite sets of values (v_l, v_t) which reproduce the frequency of the first breathing mode. Figure 20 represents the couple of transverse and longitudinal velocities compatible with a fundamental breathing mode frequency equal to 15.6 GHz measured in a copper single nanowire exhibiting a radius of 91 nm [109]. This curve clearly underlines the lack of experimental information to get a complete elastic characterization.

Consequently, in order to assess the validity of the classical continuum theories at the nanoscale [110, 111], we have to consider alternative measurements to get a better elastic characterization.

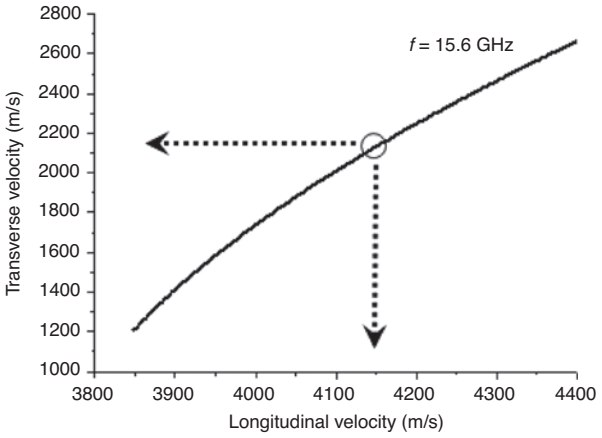

Figure 20: Black curve corresponding to the different couples of v_l and v_t which give the first breathing mode frequency equal to 15.6 GHz obtained in 91 nm diameter single copper nanowires [109]. The black arrow pointed out the standard velocities in polycrystalline copper around 4150 m.s^{-1} and 2150 m.s^{-1}, respectively, for longitudinal and transverse sound velocity.

The first method considered is to increase the quality factor of the nanowire resonance. In other words, the elastic energy must be confined into the nanostructure by suppressing any mechanical coupling, especially with the substrate holder. Experimentally, this is achieved by investigating freestanding nanostructures. In order to reduce the influence of the silicon substrate on the vibrational landscape, the wires are dispersed on a Si wafer or glass substrate which has been preliminary structured with periodic trenches using a standard optical lithography system [109, 112]. The main advantage of such free geometry is the possibility to compare on the same nanowire the time-resolved acoustic signatures measured on a supported area and its freestanding counterpart.

Figure 21 presents this comparison in Au40% – Ag60% alloy nanowires showing different frequency signatures. Recently, experiments performed in reflectivity geometry have demonstrated that the low frequency component, around 1.7 GHz, could be treated with the Hertz contact theory [104], the high frequency component being related to the breathing resonance, at 13.4 GHz in the present case. Obviously, the low frequency features disappeared in the freestanding response, but an additional peak appears at a higher frequency value of 32.2 GHz. This extra peak is associated with the first breathing harmonic mode. Concomitantly, the quality factor of the fundamental mode increased which demonstrates a better elastic confinement into the nanowire.

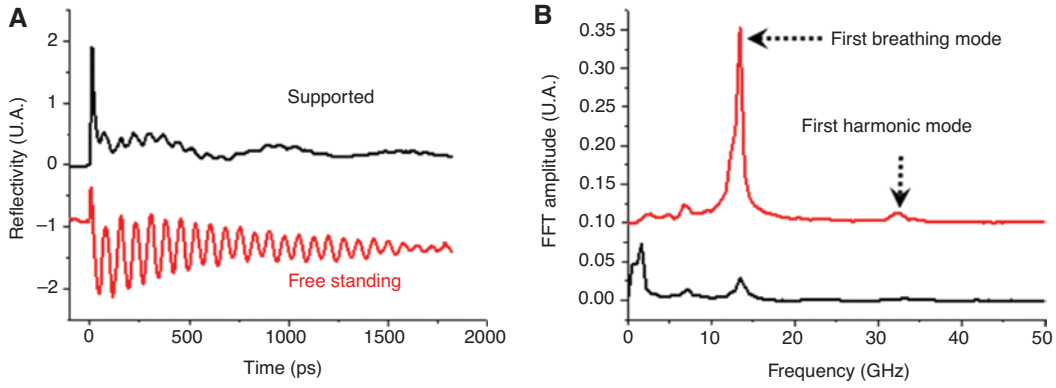

Figure 21: Phonons in supported and free standing single nanowire.
(A) Comparison of transient reflexivity of a single Au40% – Ag60% supported or in free standing geometry. (B) Fast Fourier transform exhibiting different vibrational responses. The signature of the fundamental breathing mode is larger and the first harmonic (32.2 GHz) is clearly visible in the suspended area while the contact mode is only visible where the nanowire is in interaction with the substrate.

Indeed, in a supported nanowire, a quality factor of the fundamental breathing mode around 17 may be deduced in comparison with 34 for their freestanding counterpart. The quality factor of the first harmonic mode is similar. In such conditions, the silicon substrate has an equivalent contribution to the apparent nanowire damping than the nanowire itself. Such low quality factor even in a suspended zone is a clear indication that the intrinsic attenuation in such granular systems is much higher than in pure metal. In comparison, quality factors around 80 up to 130 in suspended pure copper nanowire have already been reported in similar experiments where first and second harmonics of the fundamental breathing mode were evidenced [30].

On the other hand, recent measurements performed on glass substrate reported weak influence in the time resolved nanowire response [113]. In such investigations, the lifetimes of the breathing modes have been measured in air and liquid surroundings to give access to high frequency viscoelastic effects.

From this multiple vibrational behaviors, one can expect to determine the three unknown nanowire properties (a, v_l, v_t) by solving this nonlinear inverse problem. However, it does not matter how many breathing mode frequencies are experimentally determined because Eq. 2 is a homogeneous function of order zero; (λa, λv_l, λv_t) or (a, v_l, v_t) with $\lambda \neq 0$, are possible solutions and there is no uniqueness.

Of course, if the radius a, can be determined using SEM or atomic force microscopy, the two first breathing modes frequencies are sufficient to completely determine the velocities, equal to $v_l = 3630$ m.s^{-1} and $v_t = 1380$ m.s^{-1} for longitudinal and transverse waves, respectively, for $a = 98$ nm Au40% – Ag60% alloy nanowire radius (Figure 22). These values are close to the Ag properties.

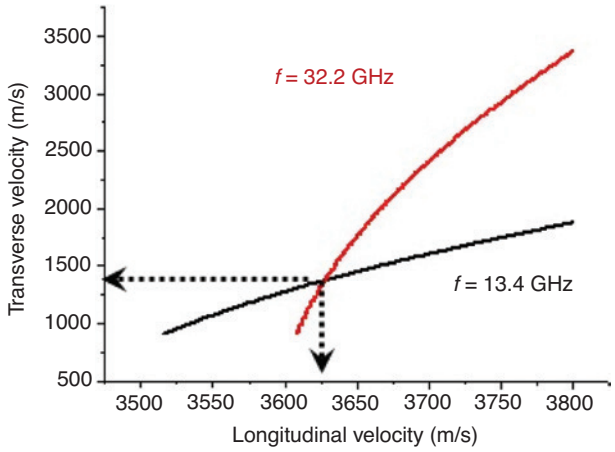

Figure 22: The black curve represents the (v_t, v_l) couple of velocity which reproduce the fundamental mode at 13.4GHz and the red curve the similar (v_t, v_l) couple associated to the second feature at 32.2 GHz. The crossing point give a self-consistent elastic characterization for a single nanowire.

However, finding a single nano-object previously studied by PU under SEM is a very tedious and often unfruitful task. Consequently, a new method to characterize completely the material and geometrical properties of nanowires with picosecond acoustic measurement remain to be found.

6.2 Propagating modes

In a similar way to what has already been done in a bundle of 75 nm GaN nanowires [23], we can consider not to be limited to the resonant modes ($q = 0$), but also to study guided acoustic modes along the nanowire axis. In parallel, guided acoustic phonons within nanowires are

emerging as promising candidates for nanoacoustic wave generation with a nanoscale spot size, which could prove useful to design nanodevices for 3D noninvasive ultrasonic imaging with nanometer resolution [114].

In order to address propagation features, a pump and probe experimental setup on a single nanowire with variable pump and probe separation was developed [30, 115]. The main idea is to follow the evolution of the acoustic signature according to the distance from the detection spot to the pump epicenter. The first results obtained are related to the propagation of the main acoustic signature, namely the breathing mode in copper nanowires. In solving the Pochhammer-Chree equation, the dispersion curve of the first breathing mode could be calculated. For wave vector smaller than 6 μm^{-1}, the dispersion curve of this mode could be approximated to a parabolic curve for 200 nm copper nanowire diameter. The quadratic coefficient, deduced experimentally, makes it possible to establish a new relation coupling the three unknown parameters of the problem [30].

In addition, this new experimental geometry allowed us to detect an acoustic mode which could not be observed with the pump and probe superimposed. This additional guided mode is characterized by a longitudinal displacement and a small radial component for a high wave vector, which explains its absence on conventional measurements. The propagation velocity c_0 of this mode deduced from the experiments can be directly correlated to the Young's modulus, assuming the density is known, as $c_0 = (E/\rho)^{1/2}$. This last information is crucial because it gives a unique opportunity to know the Young's modulus without having to know the diameter of the wire. We obtain here an equation, which directly links the two sound velocities without needing additional dimensional information.

Figure 23 shows the different sound velocities able to reproduce the frequency position of the different vibration modes as well as the value of the Young's modulus in a copper nanowire [30]. We can notice that a common waypoint is only feasible for a precise and unique value of the nanowire radius. Finally, measuring $c_0 = 3600$ m.s^{-1}, $f_{B1} = 15.6$ GHz, and $f_{B2} = 39.6$ GHz gives $a = 91 \pm 3$ nm, $v_l = 4100 \pm 200$ m.s^{-1}, and $v_t = 2200 \pm 100$ m.s^{-1}.

In summary, by considerably reducing the relaxation channel toward the substrate, the suspended nanowires provide a unique tool to observe the propagation of gigahertz guided acoustic waves. Therefore, this relaxation mechanism must be taken into account in the energy balance, which is rarely done. Taking advantage of the expression given in Ref. [29], the upper limit of the quality factor in suspended 200-nm copper single nanowire associated with these guided coherent phonons may be

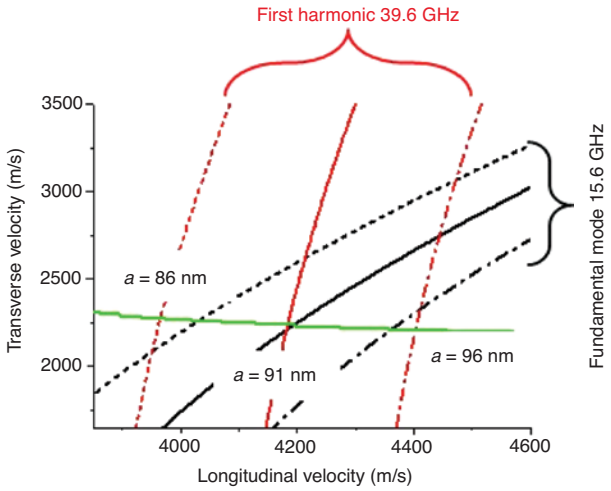

Figure 23: The black and red curves give the sound velocity compatible with the resonance frequencies of first (15.6 GHz) and second (39.6 GHz) breathing modes respectively, and the green curve is deduced from the Young's modulus equal to 116 GPa [30]. These measurements have been performed in polycrystalline copper nanowire. Only the set of curve computed with $a = 91$ nm are able to reproduce simultaneously all the experimental results.

estimated to around 200. At the same time, different harmonic modes could be observed. Coupling all this information, a complete elastic and shape characterization may be achieved in a single nanowire.

Beyond this new way to achieve material and geometrical characterization through picosecond acoustic experiment, this study paves the way to use nanowires as acoustic transducers with nanoscale lateral size. Indeed, we just described, with the propagation of guided modes, a process of acoustic energy relaxation into a nanowire. Nevertheless, the relaxation through the contact between a nano-object and the substrate is another possible phenomenon which was very quickly evoked leading to the observation of low quality factor resonances [76]. Such coupling between a silicon substrate and a gold nanostructure obtained by lithography has been recently tuned in order to create an efficient bulk transverse wave emitter with tunable frequency [115]. Although this assumption was mentioned very early it was necessary to wait for recent work [116], for a direct demonstration of acoustic wave emission assisted by an individual nanowire.

Monochromatic and geometrically anisotropic acoustic fields generated by 400 and 120 nm diameter copper nanowires simply dropped on a 10-μm silicon membrane have been investigated in transmission using 3D time-resolved femtosecond pump-probe experiments. Two pump-probe time-resolved experiments are carried out at the same time on both sides of the silicon substrate. In Figure 24A, standard experiments allowed to confirm the

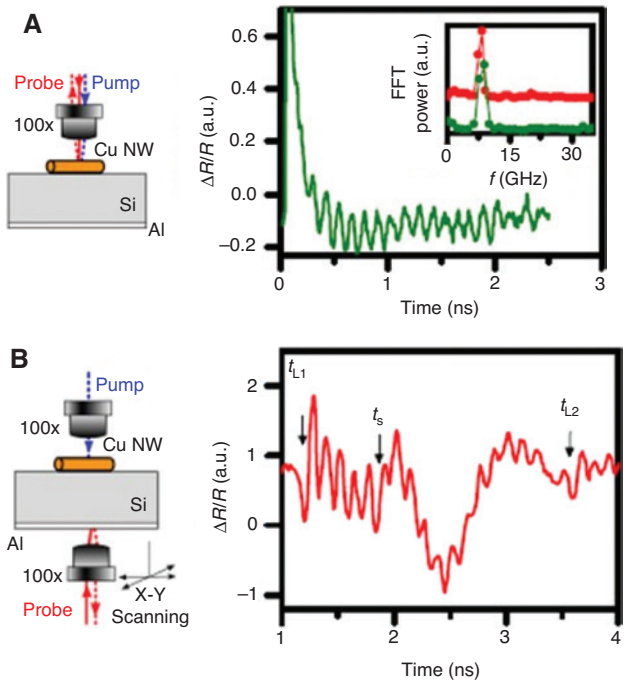

Figure 24: Acoustic field emitted by a single nanowire. (A) Schematic experimental geometry in standard front side experiment. The green curve presents the vibrational response of 400 nm copper nanowire diameter. The FFT insert curve gives an eigenmode at around 8 GHz, exactly superimposed on the FFT response measured at the opposite surface. (B) Schematic experimental geometry in back side experiment. The red curve presents the vibrational response emitted by the nanowire emerging after $t_{t1} = 1.2$ ns at the second free surface [116]. Reproduced with permission [116]. Copyright (2016) American Chemical Society.

breathing mode excitation exhibiting low quality factor while it can be seen on Figure 24B that a transmission experiment could detect the acoustic field emitted by the nanowire.

After a delay of around 1.2 ns corresponding to the travel time of a longitudinal wave in the silicon membrane, we observed an oscillating signature at a frequency equal to the nanowire's eigenmode. These results unequivocally prove that a nanowire could be assimilated to a nanometric acoustic source of longitudinal acoustic bursts with a tunable frequency in the tens of GHz range. Additional surface displacement mapping of the acoustic field produced by a single nanowire has revealed anisotropic emission due to the elongated acoustic source. Using a specific optical geometry, a net anisotropy of the acoustic field has been evidenced and correlated to the source orientation [116]. Other investigations could also involve such a nanoscale transducer to pave the way to acoustic microscopy with nanoscale lateral resolution if they could be implemented in a scanning device.

7 Conclusions and perspectives

The study of the phononic properties of nanowires is still a burgeoning field that requires technical developments to be fully understood. However, in the span of a few years, great progress has been made that now provides a clearer picture of phonons behavior in these structures. First, we have seen that the study of resonant modes of nanowires can be performed. In particular, we showed that by tuning the experimental conditions, various modes are accessible. Propagating modes were also successfully observed in both standing nanowires or lying on a substrate. Further analysis and characterization have been enabled thanks to these observations. For instance, the detection of multiple phonon frequencies allowed to determine the elastic properties of the constituting material, but also find the dimensions of the nanowire.

We also had a glimpse of the future of research on phonons in nanowires. For instance, motivated by the need for efficient thermoelectric materials, further reduction of the thermal conductivity in nanowires is needed. Thanks to the opportunity given by the presented experimental methods to observe the wave nature of phonons, coherent approaches to reduce thermal conductivity, based on phonon interferences and the opening of phononic bandgaps, can be developed and characterized. The possibility to use nanowires as tunable sources of acoustic phonons is also the first step towards high resolution three-dimensional acoustic imaging. Such techniques would then allow the non-destructive investigation of nanoscale embedded structures. Finally, the interaction of photons and phonons in nanowires is strongly modified compared to bulk materials. The central role that phonons play in defining material properties could be used to develop nanowire-based materials with novel electronic and photonic properties by tailoring their interactions with phonons.

References

[1] Dasgupta NP, Sun J, Liu C, et al. 25th Anniversary article: semiconductor nanowires – synthesis, characterization, and applications. Adv Mat 2014;26:2137–84.
[2] Wallentin J, Anttu N, Asoli D, et al. InP nanowire array solar cells achieving 13.8% efficiency by exceeding the ray optics limit. Science 2014;339:1057–60.
[3] van Dam D, van Hoof NJJ, Cui Y, et al. High-efficiency nanowire solar cells with omnidirectionally enhanced absorption due to self-aligned indium–tin–oxide mie scatterers. ACS Nano 2016;10:11414–9.

[4] Cui Y, Lieber CM. Functional nanoscale electronic devices assembled using silicon nanowire building blocks. Science 2001;291:851–3.
[5] Palacios T. Nanowire electronics comes of age. Nature 2012;481:152–3.
[6] Hällström W, Mårtensson T, Prinz C, et al. Gallium phosphide nanowires as a substrate for cultured neurons. Nano Lett 2007;7:2960–5.
[7] Patolsky F, Zheng G, Lieber CM. Nanowire sensors for medicine and the life sciences. Nanomedicine 2006;1:51–65.
[8] Jacobsson D, Panciera F, Tersoff J, et al. Interface dynamics and crystal phase switching in GaAs nanowires. Nature 2016;531:317–22.
[9] Borgström MT, Wallentin J, Trägårdh J, et al. In situ etching for total control over axial and radial nanowire growth. Nano Res 2010;3:264–70.
[10] Heiss M, Fontana Y, Gustafsson A, et al. Self-assembled quantum dots in a nanowire system for quantum photonics. Nat Mater 2013;12:439–44.
[11] Mourik V, Zuo K, Frolov SM, Plissard SR, Bakkers EPAM, Kouwenhoven LP. Signatures of majorana fermions in hybrid superconductor-semiconductor nanowire devices. Science 2012;336:1003–7.
[12] Li M, Tang HX, Roukes ML. Ultra-sensitive NEMS-based cantilevers for sensing, scanned probe and very high-frequency applications. Nat Nanotech 2007;2:114–20.
[13] Chen IJ, Burke A, Svilans A, Linke H, Thelander C. Thermoelectric power factor limit of a 1D nanowire. Phys Rev Lett 2018;120:177703.
[14] Schmid H, Borg M, Moselund K, et al. Template-assisted selective epitaxy of III-V nanoscale devices for co-planar heterogeneous integration with Si. Appl Phys Lett 2015;106:233101.
[15] Lee H-Y, Shen T-H, Hu C-Y, Tsai Y-Y, Wen C-Y. Producing atomically abrupt axial heterojunctions in silicon-germanium nanowires by thermal oxidation. Nano Lett 2017;17:7494–9.
[16] Mante P-A, Stoumpos CC, Kanatzidis M-G, Yartsev A. Electron–acoustic phonon coupling in single crystal $CH_3NH_3PbI_3$ perovskites revealed by coherent acoustic phonons. Nat Comm 2017;8:14398.
[17] Bardeen J, Cooper LN, Schrieffer JR. Theory of superconductivity. Phys Rev 1957;108:1175–204.
[18] Li D, Wu Y, Kim P, Shi L, Yang P, Majumdar A. Thermal conductivity of individual silicon nanowires. Appl Phys Lett 2003;83:2934–6.
[19] Hochbaum AI, Chen R, Diaz Delgado R, et al. Enhanced thermoelectric performance of rough silicon nanowires. Nature 2007;451:163–7.
[20] Boukai AI, Bunimovich Y, Tahir-Kheli J, Yu J-K, Goddard III WA, Heath JR. Silicon nanowires as efficient thermoelectric materials. Nature 2007;451:168–71.
[21] Yang F, Grimsley TJ, Che S, Antonelli GA, Maris HJ, Nurmikko AV. Picosecond ultrasonic experiments with water and its application to the measurement of nanostructures. J Appl Phys 2010;107:103537.
[22] Lin K-H, Chern G-W, Yu C-T, et al. Optical piezoelectric transducer for nano-ultrasonics. IEEE Trans Ultrason Ferroelectr Freq Control 2005;52:1404–14.
[23] Mante P-A, Wu Y-C, Ho C-Y, Tu L-W, Sun C-K. Gigahertz coherent guided acoustic phonons in AlN/GaN nanowire superlattices. Nano Lett 2013;13:1139–44.
[24] Thomsen C, Grahn HT, Maris HJ, Tauc J. Surface generation and detection of phonons by picosecond light pulses. Phys Rev B 1986;34:4129–38.
[25] Visscher WM, Migliori A, T.Bell M, Reinert RA. On the normal modes of free vibration of inhomogeneous and anisotropic elastic objects. J Acoust Soc Am 1991;90:2154–62.
[26] Pochhammer L. Ueber die Fortpflanzungsgeschwindigkeiten kleiner Schwingungen in einem unbegrenzten isotropen Kreiscylinder. J Reine Angew Math 1876:81:324–36.
[27] Chree C. The equations of an isotropic elastic solid in polar and cylindrical coordinates, their solutions and applications. Trans Cambridge Philos Soc Math Phys Sci 1889;14:250–369.
[28] Royer D, Dieulesaint E. Elastic waves in solids i: free and guided propagation; advanced texts in physics. Berlin–Heidelberg, Springer, 1999.
[29] Garcia-Sanchez D, Déleglise S, Thomas J-L, Atkinson P, Lagoin C, Perrin B. Acoustic confinement in superlattice cavities. Phys Rev A 2016;94:033813.
[30] Jean C, Belliard L, Cornelius TW, et al. Direct observation of gigahertz coherent guided acoustic phonons in free-standing single copper nanowires. J Phys Chem Lett 2014;5:4100–4.
[31] Hladky-Hennion A-C. Finite element analysis of the propagation of acoustic waves in waveguides. J Sound Vib 1996;194: 119–36.
[32] Nishiguchi N, Ando Y, Wybourne MN. Acoustic phonon modes of rectangular quantum wires. J Phys: Condens Matter 1997;9:5751–64.
[33] Li G, Lamberton Jr GA, Gladden JR. Acoustic modes of finite length homogeneous and layered cylindrical shells: Single and multiwall carbon nanotubes. J Appl Phys 2008;104:033524.
[34] Martínez-Gutiérrez D, Velasco VR. Acoustic waves of GaN nitride nanowires. Surf Sci 2011;605:24–31.
[35] Mizuno S, Nishiguchi N. Acoustic phonon modes and dispersion relations of nanowire superlattices. J Phys: Condens Matter 2009;21:195303.
[36] Iwai Y, Mizuno S. Coherent guided acoustic phonons in GaN/AlN nanowire superlattices. Jap J Appl Phys 2018;57:07LB02.
[37] X Lü, Chu J. Lattice thermal conductivity in a silicon nanowire with square cross section. J Appl Phys 2006;100:014305.
[38] Sarrazin E, Barraud S, Bournel A, Triozon F. Electron dynamics in silicon nanowire using a Monte-Carlo method. J Phys: Conf Series 2009;193:012126.
[39] Fonoberov VA, Balandin AA. Giant enhancement of the carrier mobility in silicon nanowires with diamond coating. Nano Lett 2006;6:2442–6.
[40] Ramayya EB, Vasileska D, Goodnick SM, Knezevic I. Cross-sectional dependence of electron mobility and lattice thermal conductivity in silicon nanowires. J Comp Elec 2008;7:319–23.
[41] Ford AC, Kumar SB, Kapadia R, Guo J, Javey A. Observation of degenerate one-dimensional sub-bands in cylindrical inas nanowires. Nano Lett 2012;12:1340–43.
[42] Benatar A, Rittel D, Yarin AL. Theoretical and experimental analysis of longitudinal wave propagation in cylindrical viscoelastic rods. J Mech Phys Sol 2003;51:1413–31.
[43] Maldovan M. Phonon wave interference and thermal bandgap materials Nat Mater 2015;14:667–74.
[44] Jean C, Belliard L, Becerra L, Perrin B. Backward propagating acoustic waves in single gold nanobeams. Appl Phys Lett 2015;107:193103.

[45] Fang N, Xi D, Xu J, et al. Ultrasonic metamaterials with negative modulus. Nat Mater 2006;5:452–6.
[46] Kargar F, Debnath B, Kakko J-P, et al. Direct observation of confined acoustic phonon polarization branches in free-standing semiconductor nanowires. Nat Comm 2016;7:13400.
[47] Wolff C, Steel MJ, Eggleton BJ, Poulton CG. Stimulated Brillouin scattering in integrated photonic waveguides: forces, scattering mechanisms, and coupled-mode analysis. Phys Rev A 2015;92:013836.
[48] Hayes W, Loudon R. Scattering of light by crystals. New York, Wiley, 1978.
[49] Dil JG. Brillouin scattering in condensed matter. Rep Prog Phys 1982;45:285–334.
[50] Mante P-A, Anttu N, Zhang W, et al. Confinement effects on Brillouin scattering in semiconductor nanowire photonic crystal. Phys Rev B 2016;94:024115.
[51] Rakich PT, Reinke C, Camacho R, Davids P, Wang Z. Giant enhancement of stimulated brillouin scattering in the subwavelength limit. Phys Rev X 2012;2:011008.
[52] Anttu N, Xu HQ. Efficient light management in vertical nanowire arrays for photovoltaics. Opt Exp 2013;21:A558–75.
[53] Wang B, Leu P. Tunable and selective resonant absorption in vertical nanowires. Opt Lett 2012;37:3756–8.
[54] Chiao RY, Townes CH, Stoicheff BP. Stimulated brillouin scattering and coherent generation of intense hypersonic waves. Phys Rev Lett 1964;12:592–5.
[55] Keiser G. Optical fiber communications. In: Proakis JG, ed. Wiley encyclopedia of telecommunications, 2003.
[56] Dainese P, Russell PJ, Joly N, et al. Stimulated Brillouin scattering from multi-GHz-guided acoustic phonons in nanostructured photonic crystal fibres. Nat Phys 2006;2:388–92.
[57] Kim J, Kuzyk MC, Han K, Wang H, Bahl G. Non-reciprocal Brillouin scattering induced transparency. Nat Phys 2015;11:275–80.
[58] Bahl G, Tomes M, Marquardt F, Carmon T. Observation of spontaneous Brillouin cooling. Nat Phys 2012;8:203–7.
[59] Van Laer R, Kuyken B, Van Thourhout D, Baets R. Interaction between light and highly confined hypersound in a silicon photonic nanowire. Nat Photon 2015;9:199–203.
[60] Chen Y-C, Kim S, Bahl G. Brillouin cooling in a linear waveguide. New J Phys 2016;18:115004.
[61] Shin H, Qiu W, Jarecki R, et al. Tailorable stimulated Brillouin scattering in nanoscale silicon waveguides. Nat Comm 2013;4:1944.
[62] Merklein M, Stiller B, Vu K, Madden SJ, Eggleton BJ. A chip-integrated coherent photonic-phononic memory. Nat Comm 2017;8:574.
[63] Johnson WL, Kim SA, Geiss R, Flannery CM, Bertness KA, Heyliger PR. Vibrational modes of GaN nanowires in the gigahertz range. Nanotechnology 2012;23:495709.
[64] Ruello P, Gusev VE. Physical mechanisms of coherent acoustic phonons generation by ultrafast laser action. Ultrasonics 2015;56:21–35.
[65] Mante P-A, Huang Y-R, Yang S-C, et al. THz acoustic phonon spectroscopy and nanoscopy by using piezoelectric semiconductor heterostructures. Ultrasonics 2015;56:52–65.
[66] Tanaka H, Sonehara T, Takagi S. A new phase-coherent light scattering method: first observation of complex brillouin spectra. Phys Rev Lett 1997;79:881–4.
[67] Pezeril T, Ruello P, Gougeon S, et al. Generation and detection of plane coherent shear picosecond acoustic pulses by lasers: Experiment and theory. Phys Rev B 2007;75:174307.
[68] Devos A, Côte R. Strong oscillations detected by picosecond ultrasonics in silicon: Evidence for an electronic-structure effect. Phys Rev B 2004;70:125208.
[69] Devos A, Le Louarn A. Strong effect of interband transitions in the picosecond ultrasonics response of metallic thin films. Phys Rev B 2003;68:045405.
[70] Maris H. Animating human motion. Sci Am 1998;278:64–9.
[71] Sun C-K, Liang J-C, Yu X-Y. Coherent acoustic phonon oscillations in semiconductor multiple quantum wells with piezoelectric fields. Phys Rev Lett 2000;84:179–82.
[72] Huynh A, Perrin B, Jusserand B, Lemaître A. Terahertz coherent acoustic experiments with semiconductor superlattices. Appl Phys Lett 2011;99:191908.
[73] Mante P-A, Devos A, Le Louarn A. Generation of terahertz acoustic waves in semiconductor quantum dots using femtosecond laser pulses. Phys Rev B 2010;81:113305.
[74] Lejman M, Vaudel G, Infante IC, et al. Ultrafast acousto-optic mode conversion in optically birefringent ferroelectrics. Nat Comm 2016;7:12345.
[75] Hu M, Wang X, Hartland GV, Mulvaney P, Perez Juste J, Sader JE. Vibrational response of nanorods to ultrafast laser induced heating: theoretical and experimental analysis. J Am Chem Soc 2003;125:14925–33.
[76] Crut A, Maioli P, Del Fatti N, Vallée F. Acoustic vibrations of metal nano-objects: time-domain investigations Phys Rep 2014;549:1–43.
[77] Jerebtsov SN, Kolomenskii AA, Liu H, et al. Laser-excited acoustic oscillations in silver and bismuth nanowires. Phys Rev B 2007;76:184301.
[78] Kolomenskii AA, Jerebtsov SN, Liu H, et al. Observation of coherent acoustic and optical phonons in bismuth nanowires by a femtosecond pump-probe technique. J Appl Phys 2008;104:103110.
[79] Sakuma H, Tomoda M, Otsuka PH, et al. Vibrational modes of GaAs hexagonal nanopillar arrays studied with ultrashort optical pulses. Appl Phys Lett 2012;100:131902.
[80] Chen H-P, Wu Y-C, Mante P-A, Tu S-J, Sheu J-K, Sun C-K. Femtosecond excitation of radial breathing mode in 2-D arrayed GaN nanorods. Opt Exp 2012;20:16611–7.
[81] Mante P-A, Ho C-Y, Tu L-W, Sun C-K. Interferometric detection of extensional modes of GaN nanorods array. Opt Exp 2012;20:18717–22.
[82] Mariager SO, Khakhulin D, Lemke HT, et al. Direct observation of acoustic oscillations in InAs nanowires. Nano Lett 2010;10:2461–5.
[83] Yang S-C, Wu Y-C, Mante P-A, et al. Efficient excitation of guided acoustic waves in semiconductor nanorods through external metallic acoustic transducer. Appl Phys Lett 2014;105:243101.
[84] Yang S-C, Wei P-K, Hsiao H-H, et al. Enhanced detection sensitivity of higher-order vibrational modes of gold nanodisks on top of a GaN nanorod array through localized surface plasmons. Appl Phys Lett 2014;105:211103.
[85] Mante P-A, Lehmann S, Anttu N, Dick KA, Yartsev A. Nondestructive complete mechanical characterization of zinc blende and wurtzite GaAs nanowires using time-resolved pump-probe spectroscopy. Nano Lett 2016;16:4792–8.

[86] Jurgilaitis A, Enquist H, Andreasson BP, et al. Time-resolved X-ray diffraction investigation of the modified phonon dispersion in InSb nanowires. Nano Lett 2014;14:541–6.
[87] Arbouet A, Christofilos D, Del Fatti N, et al. Direct measurement of the single-metal-cluster optical absorption. Phys Rev Lett 2004;93:127401.
[88] Richter G, Hillerich K, Gianola DS, Mnig R, Kraft O, Volkert CA. Ultrahigh strength single crystalline nanowhiskers grown by physical vapor deposition. Nano Lett 2009;9:3048–52.
[89] Korte KE, Skrabalak SE, Xia YN. Rapid synthesis of silver nanowires through a CuCl- or CuCl2-mediated polyol process. J Mater Chem 2008;18:437–41.
[90] Toimil Molares ME, Buschmann V, Dobrev D, et al. Single-crystalline copper nanowires produced by electrochemical deposition in polymeric ion track membranes. Adv Mater 2001;13:62–5.
[91] Van Dijk MA, Lippitz M, Orrit M. Detection of acoustic oscillations of single gold nanospheres by time-resolved interferometry. Phys Rev Lett 2005;95:267406.
[92] Burgin J, Langot P, Del Fatti N, Vallée F, Huang W, El-Sayed MA. Time-resolved investigation of the acoustic vibration of a single gold nanoprism pair. J Phys Chem C 2008;112:11231–5.
[93] Staleva H, Hartland GV. Vibrational dynamics of silver nanocubes and nanowires studied by single-particle transient absorption spectroscopy. Adv Funct Mater 2008;18:3809–17.
[94] Marty R, Arbouet A, Girard C, et al. Damping of the acoustic vibrations of individual gold nanoparticles. Nano Lett 2011;11:3301–6.
[95] Kelf TA, Tanaka Y, Matsuda O, Larsson EM, Sutherland DS, Wright OB. Ultrafast vibrations of gold nanorings. Nano Lett 2011;11:3893–8.
[96] Staleva H, Hartland GV. Transient absorption studies of single silver nanocubes. J Phys Chem C 2008;112:7535–9.
[97] Zijlstra P, Tchebotareva AL, Chon JWM, Gu M, Orrit M. Acoustic oscillations and elastic moduli of single gold nanorods. Nano Lett 2008;8:3493–7.
[98] Jais PM, Murray DB, Merlin R, Bragas AV. Metal nanoparticle ensembles: tunable laser pulses distinguish monomer from dimer vibrations. Nano Lett 2011;11:3685–9.
[99] Juvé V, Crut A, Maioli P, et al. Probing elasticity at the nanoscale: terahertz acoustic vibration of small metal nanoparticles. Nano Lett 2010;10:1853–8.
[100] Vertikov A, Kuball M, Nurmikko AV, Maris HJ. Time-resolved pump-probe experiments with subwavelength lateral resolution. Appl Phys Lett 1996;69:2465–7.
[101] Siry P, Belliard L, Perrin B. Picosecond acoustics with very high lateral resolution. Acta Acust Acust 2003;89:925–9.
[102] Bainier C, Vannier C, Courjon D, et al. Comparison of test images obtained from various configurations of scanning near-field optical microscopes. Appl Opt 2003;42:691.
[103] Bienville T, Robillard JF, Belliard L, Roch-Jeune I, Devos A, Perrin B. Individual and collective vibrational modes of nanostructures studied by picosecond ultrasonics. Ultrasonics 2006;44:e1289–94.
[104] Guillet Y, Audoin B, Ferrié M, Ravaine S. All-optical ultrafast spectroscopy of a single nanoparticle-substrate contact. Phys Rev B 2012;86:035456.
[105] Guillet Y, Rossignol C, Audoin B, Calbris G, Ravaine S. Optoacoustic response of a single submicronic gold particle revealed by the picosecond ultrasonics technique. Appl Phys Lett 2009;95:061909.
[106] Hu M, Wang X, Hartland GV, Mulvaney P, Juste JP, Sader JE. Vibrational response of nanorods to ultrafast laser induced heating: theoretical and experimental analysis. J Am Chem Soc 2003;125:14925–33.
[107] Voisin C, Christofilos D, Del Fatti N, Vallée F. Environment effect on the acoustic vibration of metal nanoparticles. Phys B Condens Matter 2002;316–317:89–94.
[108] Decremps F, Belliard L, Gauthier M, Perrin B. Equation of state, stability, anisotropy and nonlinear elasticity of diamond-cubic (ZB) silicon by phonon imaging at high pressure. Phys Rev B 2010;82:104119.
[109] Belliard L, Cornelius TW, Perrin B, et al. Vibrational response of free standing single copper nanowire through transient reflectivity microscopy. J Appl Phys 2013;114:193509.
[110] Liang HY, Upmanyu M, Huang HC. Size-dependent elasticity of nanowires: nonlinear effects. Phys Rev B 2005;71:241403.
[111] Petrova H, Pérez-Juste J, Zhang ZY, Zhang J, Kosel T, Hartland GVJ. Crystal structure dependence of the elastic constants of gold nanorods. Mater Chem 2006;16:3957–63.
[112] Major TA, Crut A, Gao B, et al. Damping of the acoustic vibrations of a suspended gold nanowire in air and water environments. Phys Chem Chem Phys 2013;15:4169–76.
[113] Devkota T, Chakraborty D, Yu K, Beane G, Sader JE, Hartland GV. On the measurement of relaxation times of acoustic vibrations in metal nanowires. Phys Chem Chem Phys 2018;20:17687–93.
[114] Lin K-H, Yu C-T, Sun S-Z, et al. Two-dimensional nanoultrasonic imaging by using acoustic nanowaves. Appl Phys Lett 2006;89:043106.
[115] Amziane A, Belliard L, Decremps F, Perrin B. Ultrafast acoustic resonance spectroscopy of gold nanostructures: towards a generation of tunable transverse waves. Phys Rev B 2011;83:014102.
[116] Jean C, Belliard L, Cornelius TW, et al. Spatiotemporal imaging of the acoustic field emitted by a single copper nanowire. Nano Lett 2016;16:6592–8.